mining

MDPI

Article

Enhanced Underground Communication: A Circularly Polarized Smart Antenna with Beam Steering for Improved Coverage

Muhammad Ahsan Mahboob [1,*], Muhammad Ahsan Ashraf [1], Iqra Atif [2,*], Hajime Ikeda [3], Glen T. Nwaila [4], Amer Masood [1], Jahanzeb Qureshi [5], Bekir Genc [6], Inamullah Khan [7] and Bruce Mellado [8,9]

1 Sibanye-Stillwater Digital Mining Laboratory (DigiMine), Wits Mining Institute (WMI), University of the Witwatersrand, Johannesburg 2050, South Africa
2 School of Geography, Archaeology and Environmental Studies, University of the Witwatersrand, Johannesburg 2050, South Africa
3 Department of Systems, Control, and Information Engineering, National Institute of Technology, Asahikawa College, 2-2-1-6 Syunkodai, Asahikawa City 071-8142, Japan
4 School of Geosciences, University of the Witwatersrand, Private Bag 3, Wits, Johannesburg 2050, South Africa
5 Institute of Space Science, University of the Punjab, Quaid-e-Azam Campus, Lahore 54590, Pakistan
6 School of Mining Engineering, University of the Witwatersrand, Johannesburg, Private Bag 3, Wits, Johannesburg 2050, South Africa; bekir.genc@wits.ac.za
7 National Institute of Transportation (NIT), Risalpur, National University of Sciences and Technology (NUST), Islamabad 44000, Pakistan
8 Institute of Collider and Particle Physics, University of the Witwatersrand, 1 Jan Smuts Avenue, Braamfontein, Johannesburg 2000, South Africa
9 National Research Foundation iThemba Laboratory for Accelerator Based Sciences, Cape Town 7100, South Africa
* Correspondence: mahsan.mahboob@wits.ac.za (M.A.M.); iqra.atif@wits.ac.za (I.A.)

Abstract: The underground mining industry faces significant challenges in maintaining reliable communication due to multipath fading and physical obstructions, leading to weak signals and dead spots. This study addresses these issues by proposing a smart antenna system with circular polarization and beam steering capabilities. The system utilizes a four-element square patch array and a Butler matrix for beamforming, enabling directional signal transmission. The antenna was designed and optimized using CST simulations. The experimental results demonstrate the antenna's ability to steer beams in four directions, significantly reducing signal interference and improving coverage. The antenna achieved a bandwidth of 400 MHz (5.52–5.99 GHz) and a gain of up to 9.69 dBi, effectively mitigating polarization mismatches. The novelty of this study lies in the integration of circular polarization and beam steering into a compact, cost-effective system, specifically designed to enhance communication in underground mining environments. This solution improves both safety and operational efficiency by providing reliable communication in harsh conditions.

Keywords: underground mines; wireless communication; mining industry; smart antenna systems; circular polarization; beam steering; connectivity; coverage; signal interference

check for updates

Academic Editors: Mostafa Benzaazoua and Krzysztof Skrzypkowski

Received: 5 June 2024
Revised: 26 December 2024
Accepted: 24 January 2025
Published: 6 February 2025

Citation: Mahboob, M.A.; Ashraf, M.A.; Atif, I.; Ikeda, H.; Nwaila, G.T.; Masood, A.; Qureshi, J.; Genc, B.; Khan, I.; Mellado, B. Enhanced Underground Communication: A Circularly Polarized Smart Antenna with Beam Steering for Improved Coverage. *Mining* **2025**, *5*, 14. https://doi.org/10.3390/mining5010014

1. Introduction

Mining is an important industry in the world economy, supplying raw minerals for a variety of industries [1]. Working in an underground mining environment, on the other hand, is a difficult task, and one of the most important components of underground mining is maintaining connectivity throughout the operation. The mining industry is facing a significant challenge as a result of connectivity issues, which are having a substantial impact on miners' productivity and safety [2–4]. Until now, due to the extreme physical conditions, such as the presence of rock, water, and dust, as well as restricted access points, the underground mining environment can pose considerable difficulties for ensuring reliable connectivity [5]. Another important aspect is the dynamic nature of underground mines as it is a vast network of tunnels, shafts, and chambers that can stretch for miles. These tunnels and chambers are often deep in the earth, making it challenging to establish a stable connection with the surface. As a result, a reliable, resilient, and effective communication system is necessary for continuous connectivity in an underground mining environment [6].

Underground mine communication systems can be categorized in a variety of ways, but they are primarily divided into three categories [7,8]: (1) Communication through the Earth (C-TTE), (2) Communication through the Wire (C-TTW), and (3) Communication through the Air (C-TTA). In addition, any combination or all three of these methods can be used, which is commonly referred to as a hybrid communication system. The most common communication systems used in underground mines are two-way radio, leaky feeder, tag-based systems, and Wi-Fi, but fiber optics are also used in some large mines, each with its own set of advantages and disadvantages [9].

Even with the advancements in recent technologies in communication systems, several research studies have reported weak signals and dead spots (areas with no communication coverage) in underground mining communications [10,11]. A range of factors contribute to the occurrence of weak signals and dead zones in underground mining sites. These factors include the following: distance traveled (particularly through solid rock); interference from other electronic devices and systems operating in the same frequency range; physical obstructions such as rocks, walls, pillars, and machinery; environmental conditions like atmospheric changes, seismic activity, and geological formations; attenuation; reflection; scattering; and many more [12,13]. Weak signals and dead spots in underground mining communication might have serious consequences. These can lead to delayed emergency responses, decreased productivity, and increased safety hazards. In critical situations, such as when a worker is unable to communicate with colleagues or the surface, rescue attempts may be delayed, putting lives at risk.

1.1. Advantages of Antenna Systems in Underground Mining

The underground mine's safety and productivity are mostly dependent on monitoring and tracking various activities, such as ensuring miner and machinery location, health, and safety. Continuous advancement in mining, on the other hand, necessitates a reliable, resilient, low-cost, easy-to-deploy wireless monitoring system capable of transmitting data from the underground working area to the control room. For a reliable wireless communication system, the antenna system needs to radiate to provide maximum coverage and enhance signal strength and data rate. Apparently, the unsuitable environment and non-line-of-sight (NLOS) in the underground mine make electromagnetic signal propagation difficult due to multipath signals. To overcome the difficulty of multipath signals, antenna systems must be designed to give higher coverage, reduced interference, and fewer multipath signals [14].

As shown in Figure 1, the omnidirectional antenna radiates electromagnetic energy in all directions, increasing signal interference due to the reflection and diffraction of signals transmitted towards the tunnel walls. The majority of the antennas now used in underground mines have an omnidirectional radiation pattern, radiating energy in all directions, including those where radiation is not required, such as towards the tunnel wall [15], whereas directional antennas radiate electromagnetic energy exclusively in the required directions, increasing the coverage area of the wireless communication system [16,17].

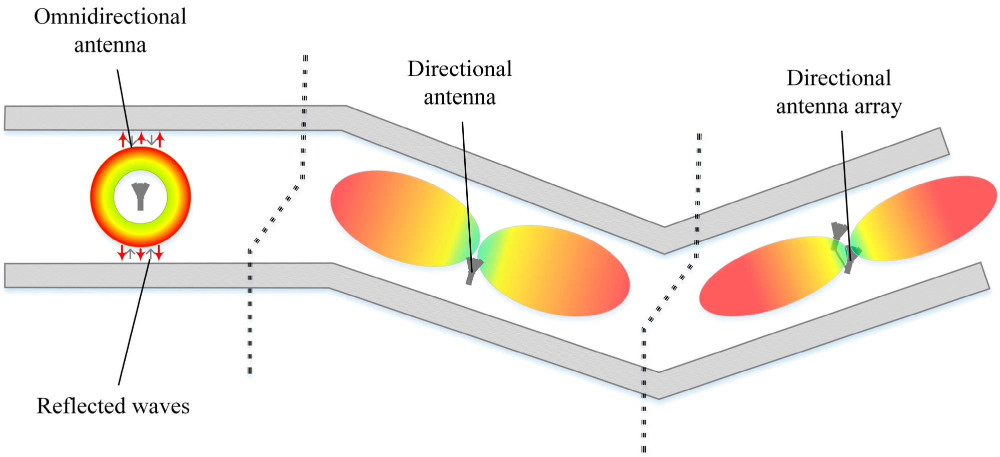

Figure 1. Radiation pattern of different antenna systems, where denser colors represent higher radiation intensity and lighter colors indicate lower radiation intensity.

Another significant challenge of wireless communication in underground mines is signal strength loss. Most antennas used in mining are linearly polarized, resulting in polarization mismatch of signals between the sending and receiving antennas [18]. As a result of the polarization mismatch, the receiving antenna receives only partial signals. As a result, building a circularly polarized (CP) antenna is an appropriate technology for reducing polarization mismatches. Furthermore, when compared to single-element antennas, adopting a directional array antenna increased the gain and signal strength of the communication established in underground mines [19,20].

With the proliferation of applications and wire-free communication devices in underground mines, the requirement for high data speeds has skyrocketed. Additionally, high-data-rate communication in underground mines is possible by boosting coverage area, signal intensity, and, eventually, multipath fading [21]. As a result, planning and considering the antenna system is critical for improving the performance of underground communication networks.

1.2. Types of Antenna Systems Used in Underground Mining

In underground mines, multipath fading is a major factor that degrades communication quality. Multipath fading occurs when a transmitted signal travels through numerous pathways to the receiver; it might interfere with itself, resulting in signal attenuation or cancelation [22]. The multipath fading can be reduced by optimizing the antenna structure and characteristics of the radiated electromagnetic signal to interact constructively with the surrounding environment and generates fewer multipath signals [23]. Different antennas were proposed for different applications in underground mines to reduce multipath fading and enhance the coverage area, as discussed below. Low-profile directional antennas and smart antenna systems such as Butler matrices are employed to improve gain and reduce the impact of multipath fading by focusing signals in desired directions [24]. Furthermore, the use of adaptive beamforming techniques in these antennas has been shown to further minimize the detrimental effects of multipath and enhance communication reliability in underground environments [25].

1.2.1. Reconfigurable Antennas

Reconfigurable antennas are those that can be adjusted in real time to maximize performance in response to changing communication requirements. These antennas may adjust their frequency, radiation pattern, polarization, and other factors, making them extremely versatile and adaptable to many communication settings [26–28]. Kunsei et al. [29] investigated the performance of pattern re-configurability in a rich multipath environment using a reconfigurable and dipole antenna in a hard rock underground mine. The results suggest that re-configurability achieves between a 20% and 34% improvement in path loss and delay spread compared to fixed-beam antennas in NLOS propagation.

1.2.2. Electrically Small Antennas

Electrically Small Antennas (ESAs) are devices that transmit and receive electromagnetic waves. These antennas are typically compact in size, making them suitable for a wide range of applications [30,31]. Chandra Dash et al. [32] designed a moderately high-gain and portable ESA at 58.27 MHz, which had a multilayered semi-cylindrical shaped structure with a finite ground plane. The proposed antenna provides a gain of 3.43 dBi and measured efficiency of 92.5%, making it suitable for underground communication. Roestorff [33] presented two electrically small reactive impedance surfaces to locate miners in emergencies in underground mines. Both antennas have a high gain of 5 dBi and radiate 10 dB more power in the front hemisphere than in the rear, and are suitable as a wearable antenna for mine rescue applications.

1.2.3. Millimeter-Wave Antennas

Millimeter-wave antennas are specialized antennas that work at frequencies ranging from 30 GHz to 300 GHz. These frequencies are substantially higher than those utilized in standard wireless communication systems, which operate at frequencies below 6 GHz [34]. The usage of millimeter-wave frequencies provides various advantages, including greater data speeds, less interference, and reduced antenna diameters [35]. Laribi et al. [36] proposed a compact, high-gain, and wideband CP antenna using millimeter (mm) waves for underground communication. A multilayer pyramidal dielectric resonator antenna was responsible for the CP mechanism. The impedance bandwidth of the antenna covers the Industrial, Scientific, and Medical (ISM) band from 58 GHz to 68 GHz with a gain of 11.2 dBi and an axial ratio bandwidth of 37% in the operating band. Using substrate-integrated waveguide technology, the horn antenna was optimized for a satellite broadcast signal in the tunnel at 27 GHz [37]. The beam width was reduced by 32 degrees, and the antenna's gain was increased by 8.78 dBi [38]. Coulibaly et al. [39] designed a coplanar waveguide-fed staked dielectric resonator antenna (DRA) for millimeter waves at 62.16 GHz for underground ISM communications. The major limitation of the proposed antenna was the degradation in radiation patterns at higher frequencies. Similarly, Agouzoul et al. [40] presented a broadband and high-gain DRA at 59.55 GHz for underground communication systems. The proposed antenna structure comprises a microstrip feed, a cylindrical resonator, and multiple metallic strips on a superstrate. The simulated results provided a gain of 15.40 dBi over the bandwidths from 57 GHz to 59.55 GHz and a maximum gain of 16.71 dBi at 58 GHz. In another study, Chorfi et al. [41] designed a cylindrical DRA two-element array at 60 GHz mounted on a conformal ground plane substrate for millimeter-wave underground communications [42].

1.2.4. Radio Frequency Identification (RFID) Antennas

RFID antennas are intended to broadcast and receive radio waves in order to communicate with RFID tags. When these tags come within range, they include miniature microchips that may store data and transmit it back to the antenna. RFID antennas are normally built of metal or conductive material and are available in a variety of shapes and sizes [43,44]. Hautcoeur et al. [45] designed an RFID tag antenna at 915 MHz for underground localization applications. A miniaturization of 31% in antenna size was achieved, and they analyzed the substrate selection for antenna efficiency. Chen and Elsherbeni [46] proposed a CP antenna for a RFID tag to be implemented in an underground localization system. The fully covered ground plane makes the tag robust due to less interaction with the attached medium. The extended metal plate provides a wide bandwidth of 37 MHz and axial ratio bandwidth of 6.4 MHz with a reading range of 2.2 m.

1.2.5. Multiband Antennas

Meng et al. [47] designed three microstrip antenna for coal mining applications. The first antenna consists of five branches, and the size and position of all of the branches was optimized. The second antenna was optimized by adding an inverted L-shaped branch on the top of the trident antenna, whereas the third antenna consists of an inverted L-shaped structure in the ground plane. The simulated and measured results cover the frequency bands of 2.51–2.68, 3.40–3.60, and 4.80–4.90 GHz. Chaouche et al. [48] proposed a novel dual-band antenna design using a genetic algorithm for ISM bands covering 2.45 GHz and 5.8 GHz. The AMC reflector consists of sixteen unit cells and is used to improve the antenna radiation characteristic and reduce the absorption of electromagnetic radiation in the human body. Kamil et al. [49] presented an ultra-wideband (UWB) antenna for under-ground UWB applications. The antenna has a patch ring and is fed with a coplanar waveguide. The antenna was optimized to achieve a bandwidth from 2.8 GHz to 12 GHz. The proposed antenna can be used for UWB applications in the underground environment, since UWB exhibits attractive merits such as wide bandwidth, simple structure, low cost, and easy fabrication.

1.2.6. Wearable Antennas

Wearable antennas are small, light antennas that can be embedded in wearable devices. They are built to receive and broadcast signals, allowing for the wearable devices to communicate with other devices like smartphones or Wi-Fi routers. Metals and conductive textiles are two commonly materials that can be used to make wearable antennas. Habani et al. [50] proposed a wearable off-body antenna based on artificial magnetic conductor frequency selective surface (AMC-FSS) at 5.8 GHz for underground communication. The antenna has three layers, an AMC substrate, a planar monopole, and a FSS super substrate, and achieved a bandwidth of 1 GHz with a directivity of 54.9°. In another study, Habani, et al. [51] improved the antenna's gain and directivity, achieving a band-width of 1.5 GHz with a directivity of 40.7°.

However, in addition to the research that has been conducted in designing antennas for effective communication and, ultimately, improved coverage, there are several issues that still require extensive research in designing an antenna system that should be efficient while posing minimal signal and coverage loss in underground mines. To overcome these challenges, smart antennas (critical components of communication systems) that can adapt to changing conditions in the underground mining environment must be developed. Modern wireless communication systems rely on multi-beam antennas to optimize their performance and achieve the desired output. These antennas have diverse applications across domains such as WLANs, base stations, satellite communications, and even automotive radars. In the context of 5G communication systems, multi-beam antennas have gained paramount importance. They enable wide-angle coverage while minimizing signal interference, making them crucial for ensuring efficient and reliable wireless communication. This study introduces a novel approach by proposing a smart antenna system specifically designed to address communication challenges in underground mines. In this paper, the current communication problems in underground mines were identified. A solution was proposed based on the existing literature. A smart antenna system was proposed to improve connectivity and coverage in underground mines. The proposed antenna was designed, and different parameters were analyzed to optimize their performance. As a result, we suggest using a four-element array with beam steering features to reduce signal interference and improve communication in underground mines.

The paper is divided into sections that discuss various aspects of the investigation. Section 2 discusses the approach, antenna system design, and Butler matrix components. This section also addresses the structure and operation of each component of the Butler matrix. Section 3 contains comprehensive details about the optimized outcomes of each Butler matrix component designed at 5.8 GHz, including the hybrid coupler, crossover, and phase shifter parameters. This section also covers the antenna design transition a from rectangular to a square patch design and provides an in-depth evaluation of the antenna array using the Butler matrix. Furthermore, the proposed antenna's practical use is thoroughly investigated. Finally, in Section 4, an in-depth conclusion is offered to summarize this study's findings.

1.2.7. Comparison of Antenna Types

Table 1 provides a comparative analysis of various antenna designs, highlighting the distinct advantages and limitations of each. These factors play a critical role in determining their suitability for underground mining applications. The selection of an antenna design is determined by specific operational requirements such as data transmission rates, coverage demands, and the ability to survive harsh underground conditions.

Table 1. Comparative analysis of antenna types for underground mining communication and a summary of key features.

Antenna Type	Bandwidth	Gain	Polarization	Coverage Area	Suitability for Dynamic Environments	Complexity and Cost	Key Features	Advantages	Limitations	Suitability for Underground Mining	Key Applications
Reconfigurable	Moderate to Narrow	Moderate to High	Tunable/Varies	Adjustable	High	High (complex design and power needs)	Real-time parameter adjustment	Versatile; can adapt frequency, pattern, and polarization. Enhances path loss and delay spread. Suitable for dynamic/multipath environments.	Complex design, higher cost. Higher power consumption.	Ideal for environments requiring flexibility in changing conditions.	Dynamic multipath environments. Real-time adaptability in underground comms.
Electrically Small	Narrow to Moderate	Low to Moderate	Linear	Limited	Moderate	Low to Moderate	Compact form factor	High efficiency in small form. - Portable and easy to deploy.	Limited gain and bandwidth.	Suitable for wearable or emergency applications (due to small size).	Emergency rescue communications. Personal monitoring in cramped or confined spaces.
Millimeter-Wave	Wide	High to Very High	Circular or Linear	Limited	Low (sensitive to obstructions)	High (advanced design needed)	High-frequency operation (30–300 GHz)	High data speeds and reduced interference. Compact size at high frequencies. Effective for large-scale high-bandwidth transmissions.	Degradation of radiation patterns at higher frequencies. Sensitive to blockages.	Effective for high-bandwidth data in larger mining operations.	High-speed data transfer. Advanced automation in large underground facilities.
RFID	Narrow	Low	Circular or Linear	Localized	Moderate	Low	Communication with RFID tags	Miniaturized, robust design. Excellent for localization and tracking.	Limited reading range. Interaction with surrounding medium can degrade performance.	Suitable for tracking/positioning applications in underground mines.	Underground asset tracking. Inventory and personnel localization.

Table 1. *Cont.*

Antenna Type	Bandwidth	Gain	Polarization	Coverage Area	Suitability for Dynamic Environments	Complexity and Cost	Key Features	Advantages	Limitations	Suitability for Underground Mining	Key Applications
Multiband	Wide	Moderate	Circular or Linear	Extended	High	High (complex, multi-standard)	Operates on multiple frequency bands	Wide operational flexibility. Supports multiple standards and frequencies. Versatile in diverse communication needs.	Higher design complexity. Potentially more expensive.	Effective when multiple standards/frequencies are needed in one system.	Multi-standard comms for voice, data, sensor integration in subterranean settings.
Wearable	Moderate	Low to Moderate	Linear or Circular (varies)	Localized	High	Moderate to High	Integrated into clothing/equipment	Lightweight and portable. Good directivity for on-body communications. Ideal for real-time health/safety monitoring.	Reduced range due to body interference. Limited off-body coverage.	Ideal for miner tracking and personal safety monitoring in real time.	Wearable safety devices. Health monitoring for workers in underground operations.

2. Materials and Methods

Phased-array antenna systems, commonly referred to as multi-beam antennas, utilize multiple beam antennas to determine the direction of the beam based on the phase and its variation [52]. These antennas offer extensive coverage at wide angles and improved connectivity. The critical component of the antenna system is the beamforming network (BFN), which adjusts the phase and amplitude of the radiating elements to steer the main beam [53,54]. BFNs can be classified into two categories: digital BFNs, and RF BFNs [55]. Digital BFNs are typically employed in adaptive array systems, while RF BFNs are used in multi-beam antenna systems.

Digital BFNs often encounter challenges such as analog-to-digital offset errors, receiver imbalances, and frequency-dependent errors [56]. On the other hand, RF BFNs can be further divided into lens-based beamformers and circuit-based beamformers. Circuit-based BFNs are constructed using directional couplers, phase shifters, and crossovers as building blocks. The circuit-based BFNs are commonly used due to their simple fabrication, cost-effectiveness, lack of external feed requirement, and compact design. The circuit based BFNs can be divided into two categories based on a variable phase shifter and a fixed passive beamformer such as a Butler Matrix (BM). The variable phase shifter has high power consumption and high insertion loss, whereas the BM provides high isolation between the input and output ports [57].

The BM network is used to feed the multiple antenna array element of $N \times N$ configuration and consists of N input and N output ports. In the Butler matrix, $\frac{N}{2} log_2(N)$ 90° hybrid coupler, $\frac{N}{2}(log_2(N) - 1)$ fixed-phase shifters, and 0 dB crossovers are used to form the beam pattern. The signal from the transceiver is fed to the antenna elements by the beamforming module with a gradually changing phase difference between the output ports. This enables the beamforming operation and facilitates the transmission of the signal in various directions [52]. The block diagram of the BM with 4 inputs and outputs is shown in Figure 2. For the 4 × 4 configuration, it consists of four branch line couplers, two phase shifters, and two crossovers. Ports 1–4 are considered as input ports and 5–8 are considered as output ports connected to the antenna array.

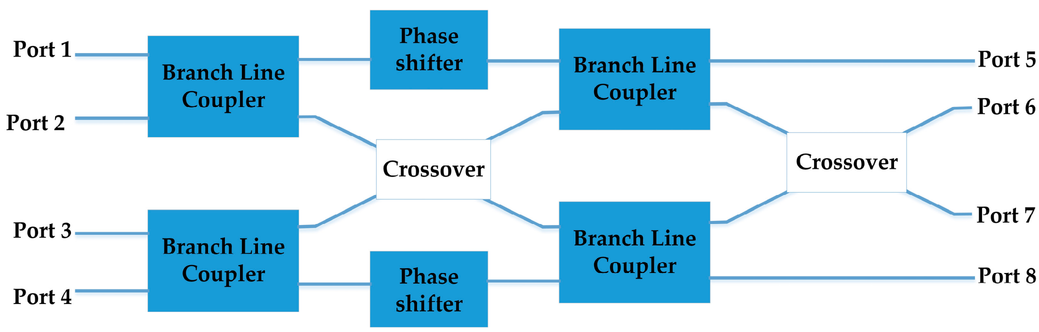

Figure 2. Block diagram of the beamforming Butler matrix network.

The BM was specifically designed for operation at 5.5 GHz, utilizing a loss-free substrate Rogers RT5880 using CST 2018 software (Dassault Systèmes, Vélizy-Villacoublay, France). This substrate possesses a relative permittivity of 2.2 and has a thickness of 0.787 mm, with a copper cladding of 0.035 mm [58,59]. The BM network, designed for four input and output ports, incorporates four hybrid couplers, two phase shifters, and two crossovers to ensure isolation between the ports. Its purpose is to generate four distinct beams located at different positions. Further explanation and the design details of each component within the Butler matrix are discussed below.

The following assumptions were made during the modeling process to ensure focus and manageability:

- The environment was considered to be homogeneous, assuming uniformity in the tunnel geometry and ignoring geological variations such as rock type differences or irregularities.
- Interference from nearby electronic devices, mining equipment, or environmental noise was not modeled, as the focus was on the antenna's beam steering performance.
- The materials used (such as the substrate Rogers RT5880) were assumed to have ideal and constant properties across all simulations.

2.1. Design of the 90° Quadrature Branch Line Coupler

The quadrature branch line coupler (BLC) is a symmetric coupler and has a 3 dB coupling factor with phase shift of 90° between the output ports [60]. The 90-degree BLCs consist of two input ports and two output ports, with a phase difference of 90 degrees be-tween the output ports. Each BLC is constructed by utilizing two horizontal and two vertical microstrip lines. These lines have a length of $\lambda_g/4$ and are characterized by respective characteristic impedances of $Z_0/\sqrt{2}$ and Z_0. The geometry of the branch line coupler is shown in Figure 3a. The BLC was designed for 5.5 GHz using the similar parameters of the substrate. The dimensions of the branch line coupler were determined using Equations (1)–(4) at 5.5 GHz [61]:

$$Z_0 = \begin{cases} \frac{60}{\in_{reff}} \, ln\left(8\frac{h}{W} + \frac{1}{8}\frac{W}{h}\right) & \frac{W}{h} \leq 1 \\ \frac{120\frac{\pi}{\in_{reff}}}{\frac{W}{h}+1.393+0.667\, ln\left(\frac{W}{h}+1.44\right)} & \frac{W}{h} \geq 1 \end{cases} \tag{1}$$

$$ZW = \left\{ \begin{array}{ll} \frac{8he^A}{e^{2A}} & \frac{W}{h} \leq 2 \\ \frac{2h}{\pi\left(B-1-ln\left(2B-1+\frac{\in_r-1}{2\in_r}\left(ln(B-1)+0.39-\frac{0.61}{\in_r}\right)\right)\right)} & \frac{W}{h} \geq 2 \end{array} \right\} \tag{2}$$

$$A = \frac{Z_0}{60}\sqrt{\frac{\in_r+1}{2}} + \frac{\in_r-1}{\in_r+1}\left(0.23 + \frac{0.11}{\in_r}\right) \tag{3}$$

$$\varepsilon_{eff} = \frac{\varepsilon_R+1}{2} + \frac{\varepsilon_R-1}{2}\left[\frac{1}{\sqrt{1+12\left(\frac{h}{W}\right)}}\right] \tag{4}$$

where W is the width of the line, h is the height of the substrate, $\in_r$ is the dielectric constant of the substrate, Z_0 is the input impedance of the port, and ε_{eff} is the effective dielectric constant. The length of the line (λ_g) is calculated using Equation (5):

$$\lambda_g = \lambda/\sqrt{\in_{eff}} \tag{5}$$

where λ the wavelength in the free space, Figure 3b is illustrates the proposed BLC.

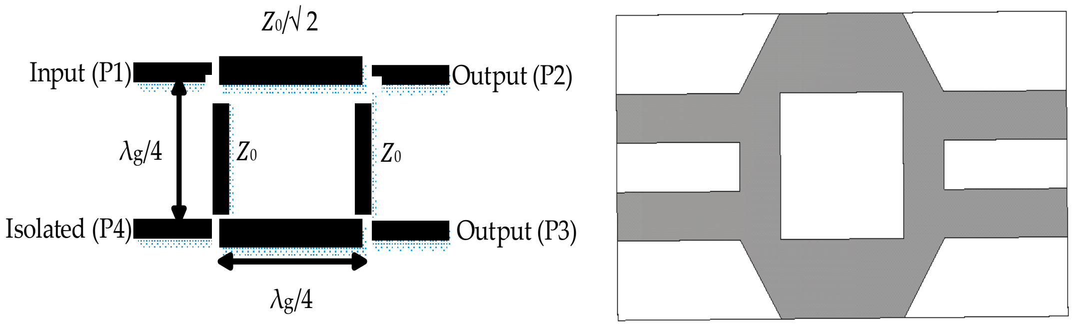

(a) (b)

Figure 3. The 90° hybrid branch line coupler's (**a**) geometric layout and (**b**) proposed layout.

2.2. Crossover Design

A crossover is a four-port network and is implemented by cascading two branch line couplers to allow for two signals to pass to the other side in the high degree of isolation and 0 dB insertion loss [53]. The geometry layout of the crossover is shown in Figure 4a. The impedance of branches are similar to BLC, except for one of the microstrip lines with the $Z_0/2$. The dimensions of all the parameters were calculated at 5.5 GHz using the microstrip equations and the same substrate parameters explained above. Figure 4b shows the proposed crossover layout for the Butler matrix.

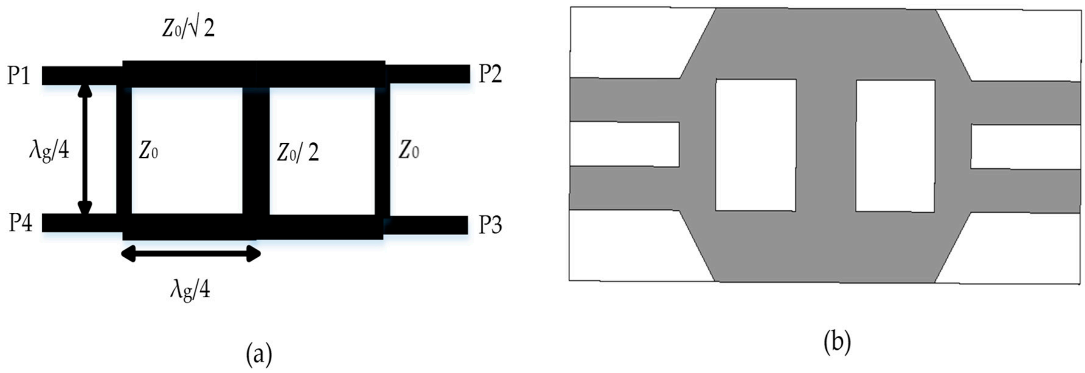

Figure 4. The 0 dB crossover's (**a**) geometric layout and (**b**) proposed layout.

2.3. Phase Shifter

The phase shifter is used to delay the phase between two lines by adding additional length to the microstrip line, as shown in Figure 5a. The length of the microstrip line is longer than the other line by $2\Delta L$. The phase shift is given by Equation (6).

$$\theta = \frac{2\pi\Delta L}{\lambda_g} \quad (6)$$

where θ represents phase shift, ΔL represents extra length of the microstrip line, and λ_g is the wavelength in the microstrip. Figure 5b illustrates the designed phase shifter for the BM network.

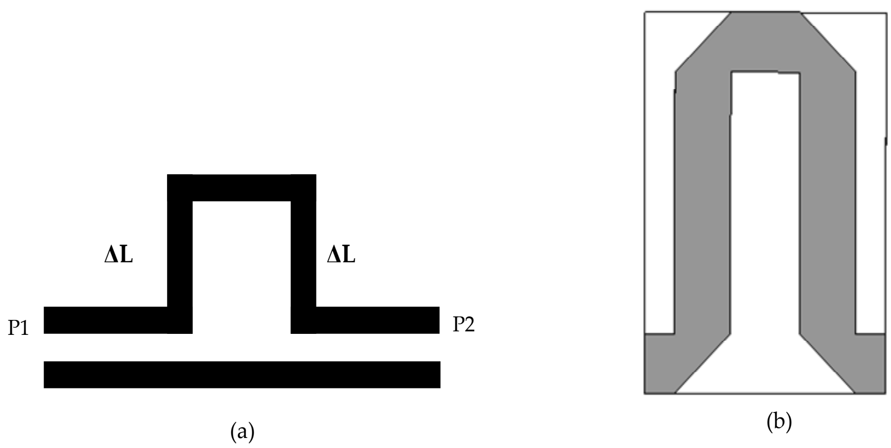

Figure 5. Phase shifter (**a**) geometry and (**b**) proposed layout.

2.4. Antenna Design

An antenna array with circular polarization and beam steering features is proposed in this article to reduce multipath fading and improve coverage and bandwidth. A circularly polarized wave reduces polarization mismatches and increases signal coverage by the reception antenna. Similarly, beam steering, as opposed to traditional antennas that radiate in all directions, can broadcast signals just toward the device, reducing multipath signals. Many studies [62–64] have emphasized the several advantages of combining circular polarization and beam steering antennas in a variety of applications; nevertheless, it has not been adequately deployed and tested in underground mines.

A single-element rectangular patch antenna with a 5.5 GHz frequency range was selected for the design and evaluation to enhance connectivity in underground mines. A single-element rectangular patch antenna is a type of antenna with a single radiating element. It is a cost-effective and simple yet effective design with significant advantages over more sophisticated antenna designs [65]. Because of its light weight and small size, this antenna has a wide range of uses in the mining industry. It may be utilized to communicate effectively between workers, equipment, and managers. These antennas can transmit and receive data, voice, and video signals, allowing for real-time communication between mine areas. In the mining industry, single-element antennas are also employed for navigation. They can be used to track the location of equipment and workers, allowing for more effective resource management and assuring safety. The 5.5 GHz frequency band, while relatively new and not as widely adopted, offers notable advantages compared to the more commonly utilized 2.4 GHz frequency range [66]. Because the 5.5 GHz frequency has a higher bandwidth, it can transmit more data at once. It also receives less interference from other devices, making it less susceptible to signal congestion and losses.

Initially, a rectangular patch antenna with a frequency of 5.5 GHz was designed by computing the length and width measurements using Equations (7)–(9) [67,68].

$$W = \frac{c}{2f_0\sqrt{\frac{\varepsilon_R+1}{2}}} \tag{7}$$

$$\varepsilon_{eff} = \frac{\varepsilon_R+1}{2} + \frac{\varepsilon_R-1}{2}\left[\frac{1}{\sqrt{1+12\left(\frac{h}{W}\right)}}\right] \tag{8}$$

$$L = \frac{c}{2f_0\sqrt{\varepsilon_{eff}}} - 0.824h\left(\frac{\left(\varepsilon_{eff}+0.3\right)\left(\frac{W}{h}+0.264\right)}{\left(\varepsilon_{eff}-0.258\right)\left(\frac{W}{h}+0.8\right)}\right) \tag{9}$$

where W is the width of the patch, ε_{eff} is the effective permittivity, ε_R is the relative permittivity of the substrate, h is the height of the substrate, L is the length of the patch, f_0 is the resonant frequency, and c is the speed of light.

The rectangular patch measures 20.45 mm in width and 17.98 mm in length. To feed an excitation signal to an antenna, the impedance of the antenna and feedline must be matched to normal impedance, i.e., 50 Ω. A matching line and a microstrip feed line with an input impedance of 50 Ω were used to power the proposed antenna. The metal traces on the patch were designed with copper annealed material and totally covered with ground on the antenna's back plane, as illustrated in Figure 6. The dimensions of the rectangular patch antenna are shown in Table 2.

Table 2. Dimensions (length and width) of the proposed rectangular patch antenna.

Parameter	Length (mm)	Parameter	Length (mm)
L	53.98	W	40.90
L1	17.98	W1	21.55
L2	10.63	W2	1.64
L3	18.61	W3	2.42
GL	53.98	GW	40.90

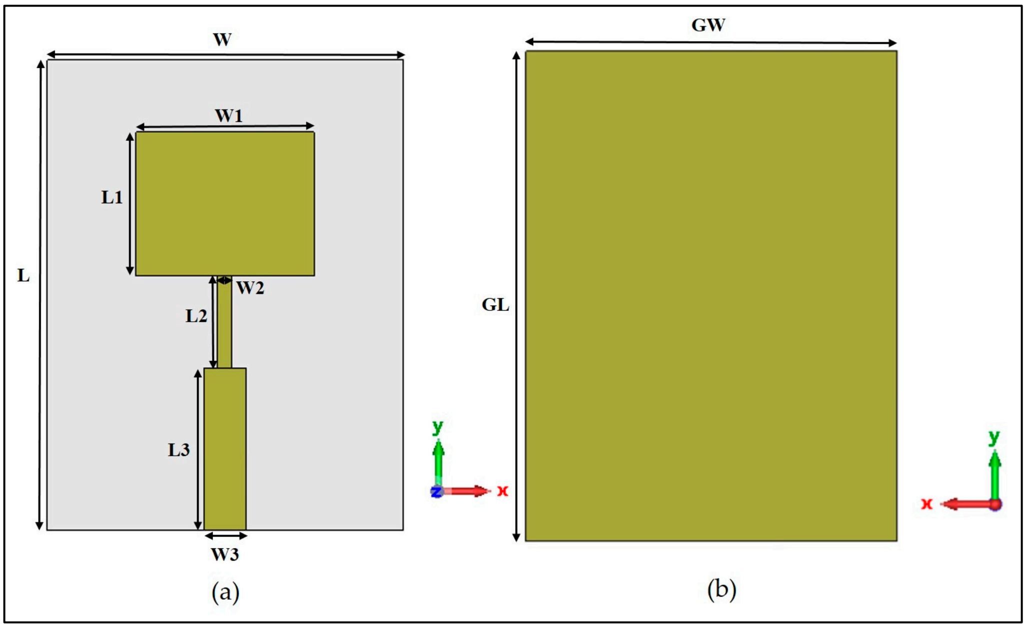

Figure 6. Schematic representation of the single rectangular patch antenna with (**a**) front and (**b**) back view.

The above designed rectangular patch antenna radiates linearly polarized wave. However, circular and elliptical polarization can be achieved using different feed arrangements or slightly modifications made to the patch antennas. A circularly polarized antenna can mitigate the polarization mismatch loss, as discussed above in Section 1.2. Therefore, it is vital to design antenna with circular polarization characteristics for underground mine communication.

Multiple studies [69–72] have described several ways for achieving circular polarization for patch antennas, including feeding at two places, creating a slot in the patch, and reducing the opposite sides of a square patch. One of the simplest techniques for achieving circular polarization and a wide bandwidth of the antenna is to trim the opposite sides of the square patch. As a result, the above-mentioned rectangular patch antenna was reshaped into a square by equal its length and width. For optimal operation at 5.5 GHz, a parametric sweep was performed on the patch width (W1). Similarly, the rectangular patch's two opposite corners were trimmed and adjusted to obtain a center frequency of 5.5 GHz. Figure 7 illustrates the proposed square patch antenna concept with trimmed edges.

Array antennas have various advantages over single-element antennas, including higher gain, increased directivity, and the ability to scan the antenna system's beam. To obtain the antenna's beam steering characteristics, an array of numerous elements must be built. As a result, a four-element linear array was designed to use for BM network for beam steering characteristics, as shown in Figure 8. The distance between elements has a significant impact on the performance of the antenna array. Hassan et al. [73] and Chen et al. [74] investigated the influence of spacing on large antenna arrays. It was discovered that 0.5λ distance produces good directivity and reduces the side lobes of the radiation. As a result, the antenna array was constructed with 0.5λ separation between each unit. The entire length of the array (A_L) was 196.76 mm, with a gap (A_G) of 27.26 mm between the two elements. The copper ground plane completely covered the array's backside.

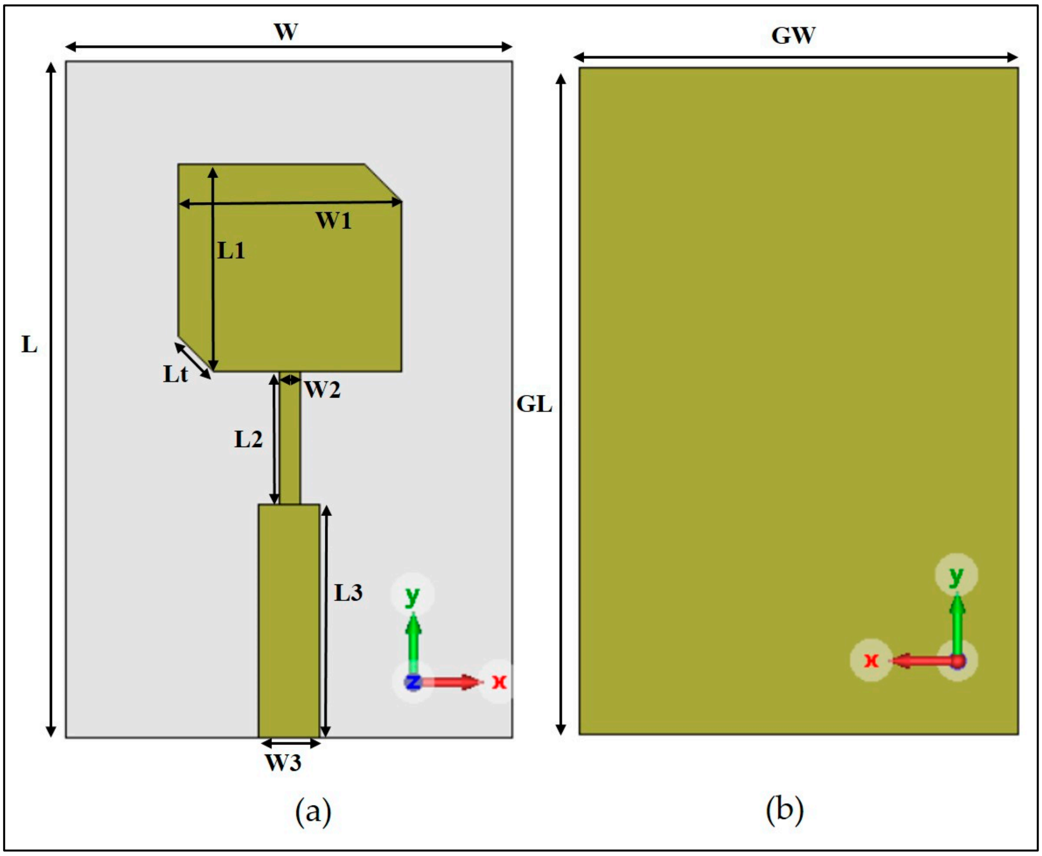

Figure 7. Schematic of the single-element square patch antenna with dimensions and (**a**) front and (**b**) back views.

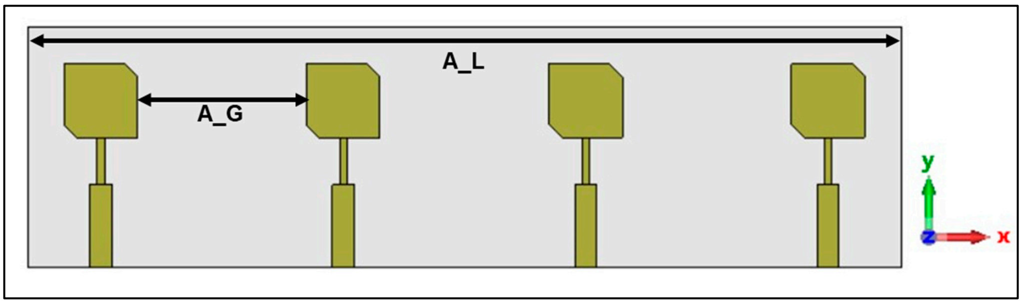

Figure 8. Structure of a square patch antenna array of a 4 × 1 element.

After setup, the final designed antenna with 5.5 GHz frequency was analyzed and optimized to achieve maximum coverage and enhanced connectivity with respect to the underground mining environment.

2.5. Butler Matrix

The performance of the Butler matrix depends on the performance of the individual parameters of each component such as bandwidth, S-parameter, isolation and insertion loss, and phase difference between the output ports. All the components were assembled to complete the Butler matrix with 4 branch line couplers, 2 phase shifts, and 2 crossovers to provide maximum isolation according to the block diagram as shown in Figure 2. The total width and length of the substrate is 159.50 mm × 130.56 mm. The array elements of the square patch antenna were attached to the output ports of the Butler matrix, as shown in Figure 9. The distance between the adjacent elements of the antenna array was kept at 0.5λ.

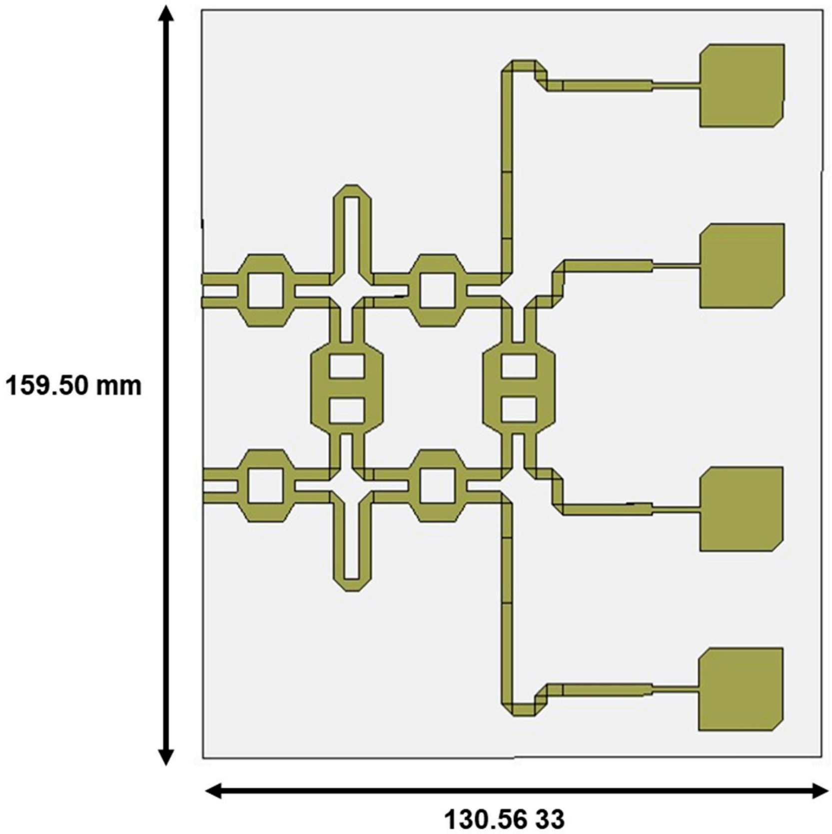

Figure 9. Butler matrix network with four elements of the antenna array.

The antenna array was simulated using CST Studio Suite within an idealized underground mining environment. Key parameters, including substrate characteristics, beam angles, and the spacing between antenna elements, were systematically adjusted to enhance performance. The system's beam steering capabilities and gain were evaluated across four distinct beams, with iterative refinements made to reduce signal reflection and maximize coverage. The simulation was conducted at an operating frequency of 5.5 GHz, selected for its lower interference and enhanced data transmission capabilities. The Rogers RT5880 substrate, with a permittivity of 2.2 and a thickness of 0.787 mm, was utilized for the antenna design. The underground mining environment was modeled as a rectangular tunnel with reflective walls, accounting for multipath signal interference. To achieve optimal gain and minimize side lobes, the antenna elements were spaced at 0.5λ within the array. The key materials and components used in the design and simulation of the antenna system, along with their physical properties and sources, are summarized in Table 3.

Table 3. Summary of sample types, physical properties, and sources used in antenna design and simulation.

Sample Type	Physical Properties	Source/Location
Rogers RT5880 Substrate	Relative Permittivity: 2.2, Thickness: 0.787 mm, Copper cladding: 0.035 mm	Manufacturer: Rogers Corporation
Antenna Array Elements	Circular Polarization, Operating Frequency: 5.5 GHz	Designed for underground mining environments
Branch Line Coupler	Length: $\lambda\_g/4$, Impedances: $Z_0/\sqrt{2}$ and Z_0, Phase Shift: 90°	Simulated using CST software
Crossover	Impedance of branches: similar to BLC, Extra line length for phase shift	Simulated in CST software
Phase Shifter	Phase Delay: −45°, Extra Line Length: 10.60 mm	Simulated in CST software

3. Results and Discussion

3.1. Hybrid Coupler

Table 4 presents the calculated and optimized dimensions of the BLC, where different parameters were varied during the optimization process. The optimized s-parameters and phase difference in the BLC are depicted in Figures 10 and 11, respectively. The results indicate that the S-parameters, specifically S_{11} and S_{14}, exhibit minimal reflection at ports 1 and 4, respectively, which indicates good impedance matching and minimal signal loss at these ports. While similar behaviors are reported in the literature by Lin et al. [75], this study extends these findings by demonstrating the optimized performance of the Butler matrix components specifically within an underground mining environment. The S_{12} and S_{13} represent the isolation of port 1 from port 2 and 3, respectively. Achieving good isolation between these ports is essential for reducing crosstalk and improving overall system performance. Similar findings are observed by Wang et al. [76] in coupled line-based millimeter-wave Complementary Metal-Oxide-Semiconductor (CMOS) power dividers, where the isolation (S_{32} and S_{23}) between output ports significantly improves system performance by minimizing interference between channels. Furthermore, Figure 10 demonstrates a phase difference of 87.27° between port 2 and port 3, which is crucial for applications requiring phase-shifted signals, such as phased-array antennas and power dividers. This phase difference is consistent with findings by Regev et al. [77], which emphasize that phase accuracy is crucial for maintaining signal coherence and beamforming performance in multi-port systems.

Table 4. Dimensions and parameters of the branch line coupler.

Parameters	Calculated	Optimized
Length (50 Ω)	9.97 mm	7.3 mm
Length (35.355 Ω)	9.82 mm	7.3 mm
Width (50 Ω)	2.42 mm	2.42 mm
Width (35.355 Ω)	3.95 mm	3.95 mm

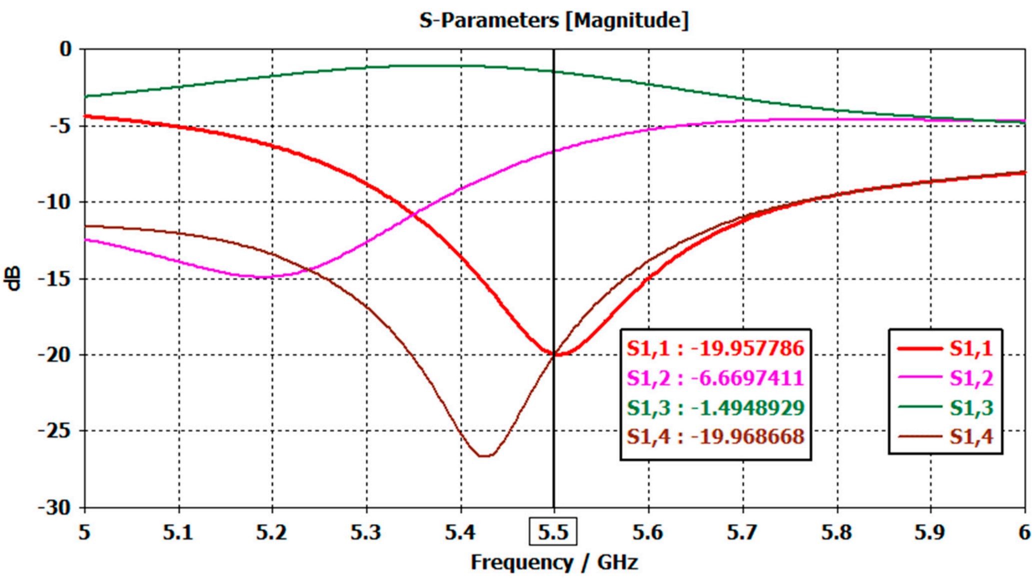

Figure 10. Magnitude of the S-parameter of the 90° hybrid BLC for input port 1.

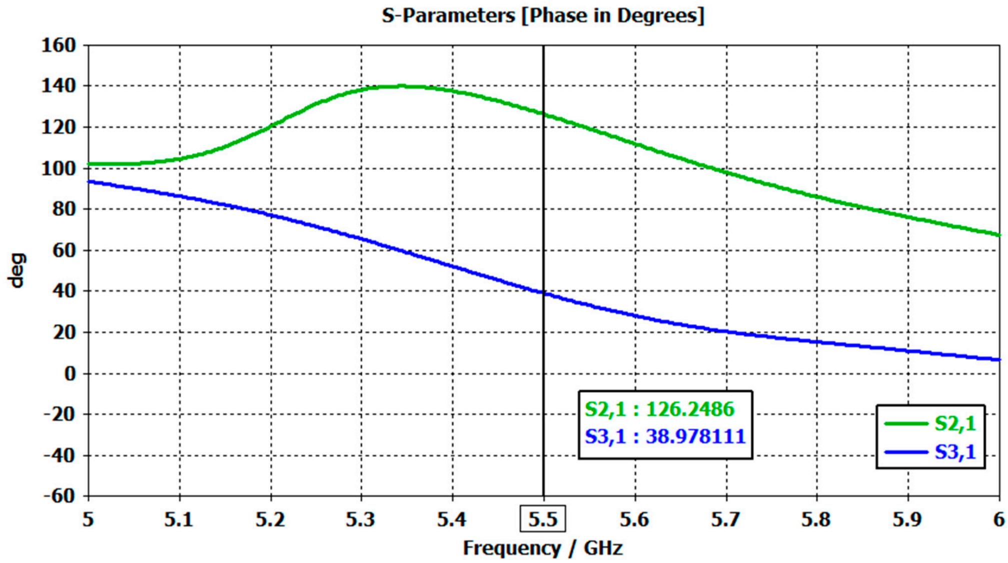

Figure 11. Phase difference in the 90° hybrid branch line coupler for input port 1.

The hybrid coupler dimensions determined in this study align with those reported previously. Building on this foundation, the work introduces a novel application by integrating the coupler into an antenna system tailored for underground mining communication. The design features a Butler matrix coupled with a circularly polarized square patch array, enhancing both signal reliability and coverage. The system achieves a bandwidth of 400 MHz and a gain of 9.69 dBi, outperforming existing designs in addressing the challenges of underground environments. Application-specific testing further validates the system's effectiveness, establishing its contribution to advancing communication technologies in mining.

3.2. Crossover

Table 5 showcases the dimensions of the crossover that were calculated and optimized using [61]. Various parameters were adjusted during the optimization process. Figure 12 shows the S-parameters of the designed crossover, which demonstrate good performance and a high level of isolation. It illustrates that the S-parameters S11, S12, and S14 exhibit minimal reflection at ports 1, 2, and 4, respectively, indicating effective impedance matching and signal transmission. These results are consistent with established optimization processes in antenna design, where minimized S-parameters are crucial for ensuring efficient signal transmission and minimizing interference, as noted by Kouhalvandi and Matekovits [78] and DiLullo et al. [79].

Table 5. Dimensions and parameters of the crossover.

Parameters	Calculated	Optimized
Length (50 Ω)	9.97 mm	7.3 mm
Length (35.355 Ω)	9.82 mm	7.3 mm
Length (25 Ω)	9.69 mm	7.3 mm
Width (50 Ω)	2.42 mm	2.42 mm
Width (35.355 Ω)	3.95 mm	3.95 mm
Width (25 Ω)	6.17 mm	4 mm

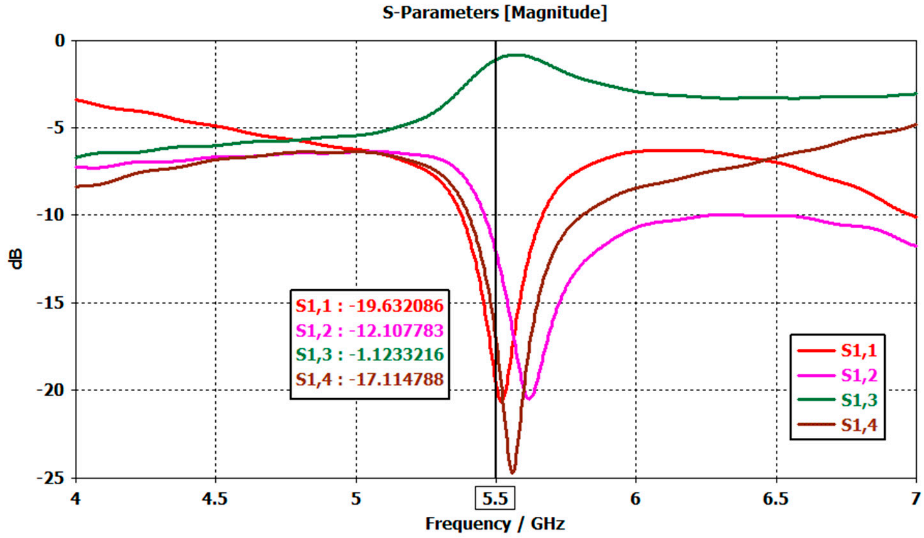

Figure 12. Magnitude of the S-parameter of the crossover for input port 1.

3.3. Phase Shifter

The phase shifter's initial calculated length was 4.6 mm, but, through optimization, it was adjusted to 10.60 mm, achieving a −45° phase shift in the line. As shown in Figure 13, the optimized phase shift in the line reached −45.8°, which is consistent with similar optimizations in phase shifters that demonstrate high accuracy and effective signal manipulation, as reported by Liu et al. [80] and Xu et al. [81].

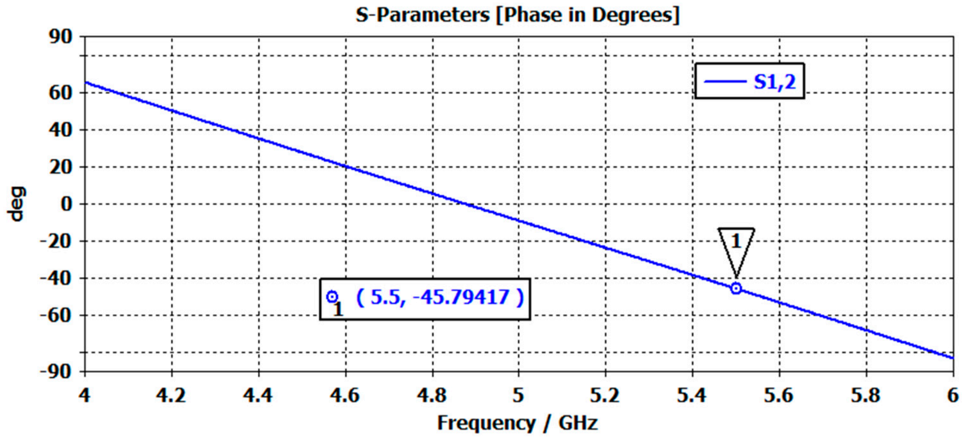

Figure 13. Phase of the S-parameter S_{12} of the proposed phase shifter.

3.4. Patch Antenna

The designed single-element square patch antenna's reflection coefficient refers to the amount of reflected signal delivered to the antenna structure in comparison to the incident signal. Generally, the reflection coefficient, known as S_{11}, indicates that the reflected signal is greater than the incident signal for port 1, and is expressed in decibels. The results suggest that, for all frequencies with S_{11} less than −10 dB, the antenna structure is regarded as radiating. This phenomenon aligns with similar findings in recent research [82,83] on patch antennas, where a reflection coefficient of less than −10 dB indicates efficient impedance matching and minimal signal loss.

Figure 14 depicts the reflection coefficient of a single rectangular patch antenna element.

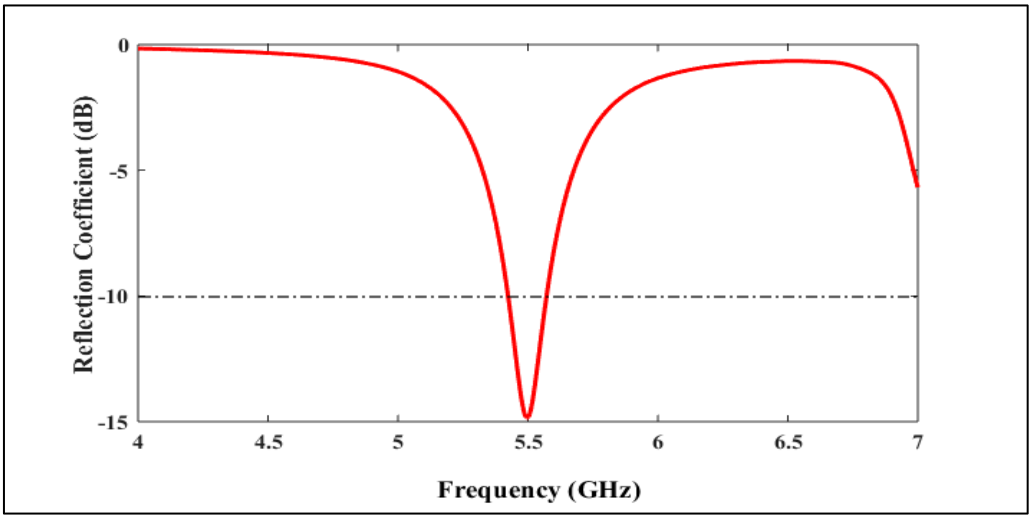

Figure 14. Reflection coefficient of single-element square patch antenna at 5.5 GHz.

The designed single-element square patch antenna has a bandwidth of 140 MHz from 5.43 GHz to 5.57 GHz, as highlighted in Figure 4, which aligns with other microstrip antenna designs that focus on achieving a wide operational bandwidth through optimization techniques [84]. Similarly, another essential antenna parameter is the far-field radiation pattern, which specifies the direction in which the antenna radiates in the far field [85]. Figure 15 depicts the designed single-element square patch antenna's cross and co-poles of the far-field radiation patterns. At 5.5 GHz, it shows a directed radiation pattern with a gain of 7.78 dBi, a gain value that is consistent with typical patch antennas of this size and configuration [86]. The rectangular patch antenna's directed radiation pattern was caused by the presence of a ground plane on its backside, as also indicated by Deshmukh et al. [87], which has been proven to significantly influence the radiation behavior by enhancing the front-to-back ratio and reducing unwanted reflections.

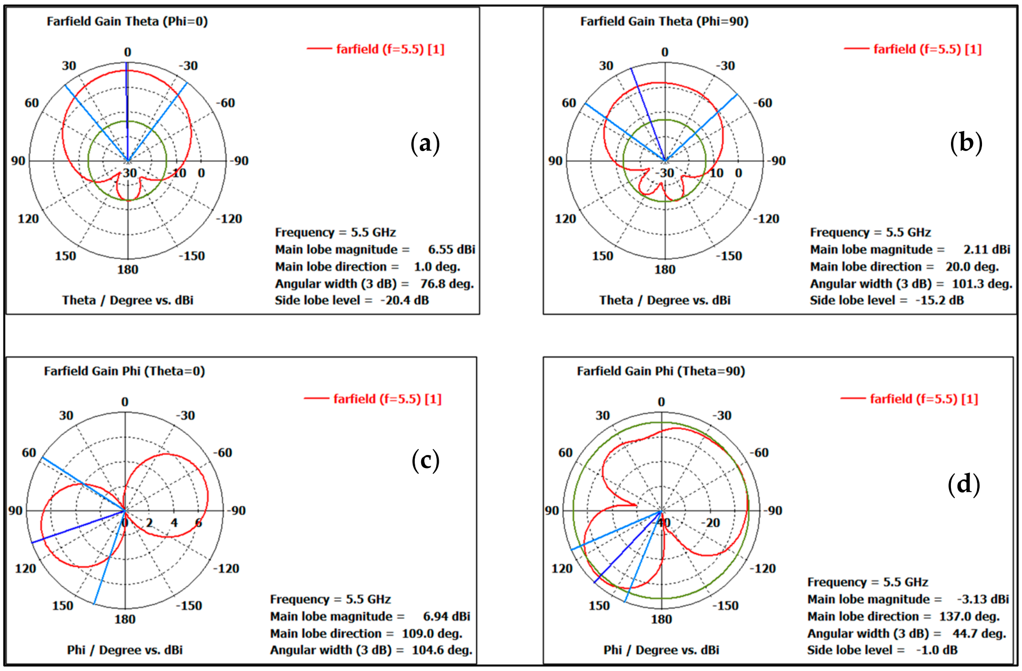

Figure 15. Far-field radiation co- and cross-pole pattern of a single-element antenna at 5.5 GHz (**a**) phi = 0, (**b**) phi = 90, (**c**) Theta = 0, and (**d**) Theta = 90.

The rectangular patch antenna was circularly polarized by changing its shape and shortening the opposite edge of the patch, which is a common technique for achieving circular polarization in patch antennas [88]. The width of the rectangular patch was reduced to create a square patch. The reflection coefficient of the square patch antenna was also displayed for various antenna widths, as shown in Figure 16. The patch's width was adjusted to 20.45 mm, 19.13 mm, 17.8 mm, and 16.5 mm. Similarly, for 0 mm to 3 mm, the parametric sweep was conducted on the reduced length of the opposing edges of the square patch. Figure 17 depicts the reflection coefficient results for the sweep analysis, a process widely used in antenna design optimization [89].

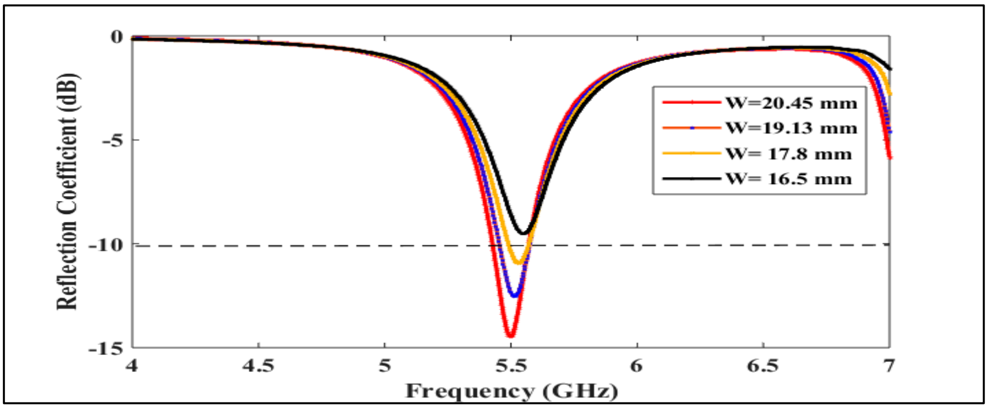

Figure 16. Reflection coefficient of parametric sweep of the width (w) of the single element antenna.

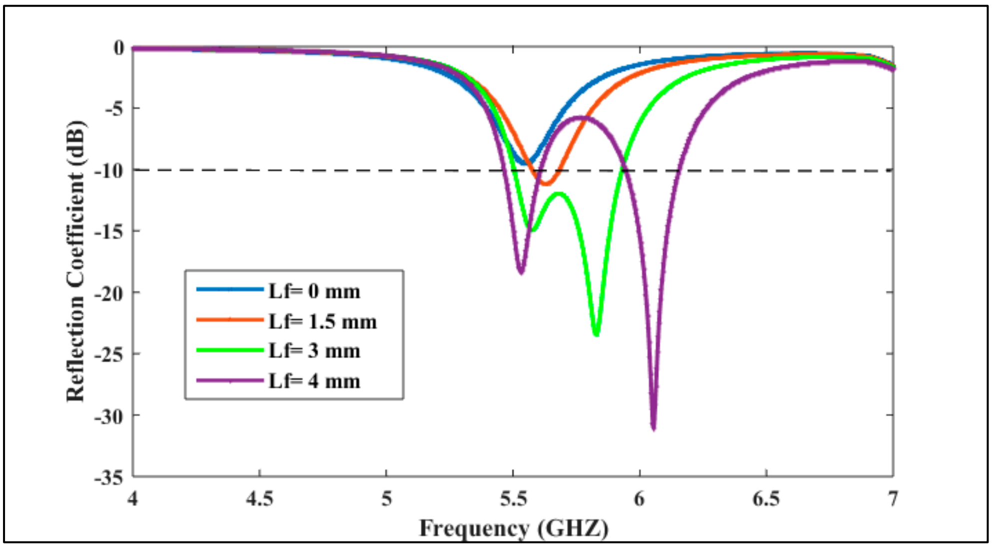

Figure 17. Reflection coefficient of the parametric sweep for the Lf length of the single-element antenna.

Figure 17 depicts the reflection coefficient results for parametric sweep analysis with different lengths of Lf (truncated length). The results show that, at Lf = 3 mm, the square patch antenna achieves a wide bandwidth, while for Lf = 4 mm, it exhibits dual-band operation with a narrower bandwidth. Therefore, the value of Lf = 3 mm was selected for the design of the square patch antenna. The final dimensions of the square patch antenna are shown in Table 6. The square patch antenna provides an impedance bandwidth of 400 MHz between 5.52 GHz and 5.99 GHz, which aligns with recent developments in circularly polarized antennas that achieve broad impedance bandwidths [90]. The single-element antenna is right-hand circularly polarized (RHCP) with a circularly polarized bandwidth of 300 MHz between 5.51 GHz and 5.81 GHz, as shown in Figure 18. Circular polarization bandwidth represents the frequency range within which the antenna radiates circularly polarized waves, a critical parameter for modern wireless communication systems [91].

Table 6. Optimized dimensions for a single-element antenna.

Parameter	Length (mm)
L	55.20
L1	17.6
L2	10
L3	10
Lf	3.0
GL	55.20
W	35.0
W1	17.6
W2	1
W3	4.91
GW	35.0

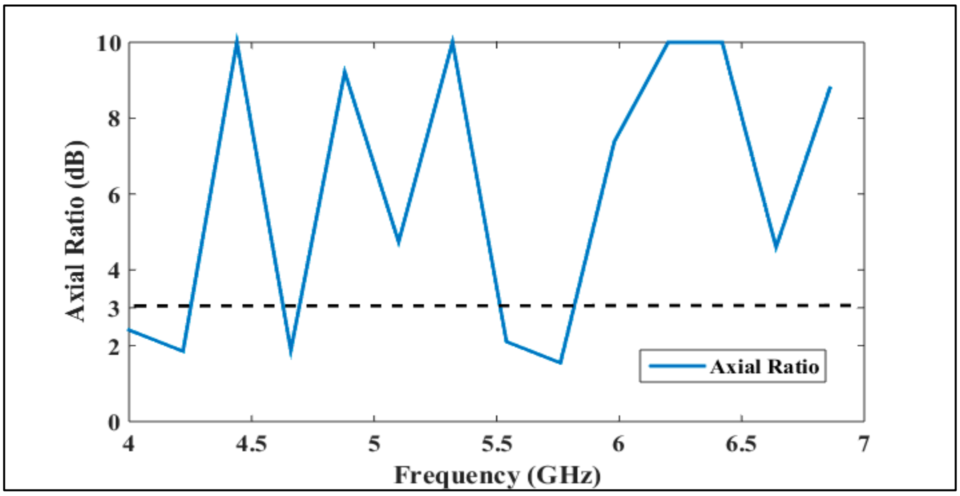

Figure 18. Axial ratio of the single-element square patch antenna.

3.5. Antenna Array with BM Network

The 4 × 4 Butler Matrix (BM) provides four distinct beams when one port is excited. For example, when one port is activated, it produces a beam at −45°, and when another port is excited, it produces a beam at 45°, with reciprocal beams for the other two ports. This behavior is consistent with previous studies that utilized the Butler Matrix for beamforming applications, where discrete beams are generated depending on the port excitation, as seen in millimeter-wave and sub-6 GHz systems [92]. The results of the BM network with the antenna array, tested at 5.5 GHz, showed consistent performance across different input ports. Figure 19 shows the return loss for port 1, port 2, port 3, and port 4, each showing minimal signal loss when only one port is excited. This aligns with established findings that demonstrate the ability of Butler matrices to maintain low return loss and high isolation between ports, which is important for ensuring efficient beam switching and steering without excessive signal degradation [93]. The far-field beam pattern, depicted in Figure 20, demonstrates the directional capabilities of the BM network. The deviation in beam angles between different ports, such as port 3 (beam at −12°) and port 4 (beam at 16°), is likely due to slight imperfections in the phase shift introduced by the Butler Matrix. This is not uncommon in practical systems, where minor phase errors can occur due to manufacturing tolerances or component mismatches, as also indicated by Jizat et al. [94]. The difference in the angles of port 3 and port 4 is due to incorrect progressive phase difference in the ports by the components of the BM network and asymmetric response of the BM network [95]. The gain of the individual beams for all ports varied between 8.38 dBi and 9.69 dBi, indicating strong directional radiation. Higher gain values suggest that the antenna efficiently directs energy into narrow beams, which is advantageous for communication systems in complex environments, such as underground mines. The variation in gain is in line with other studies that demonstrate slight differences in gain across different input ports due to phase and amplitude variations in the Butler Matrix [96] (Dong et al., 2023). This enhanced directional radiation is particularly beneficial in underground mining environments, where obstacles and signal interference are major challenges. By directing the antenna's beam towards specific angles, the system can mitigate signal reflections and improve signal-to-noise ratios, leading to better overall communication performance. Moreover, the ability to steer beams in multiple directions without physical movement of the antenna makes the system well-suited for dynamic environments where the direction of communication may frequently change. This adaptability is a key advantage of using a Butler Matrix for beamforming applications in underground mines, where traditional omnidirectional antennas may struggle with coverage and interference issues.

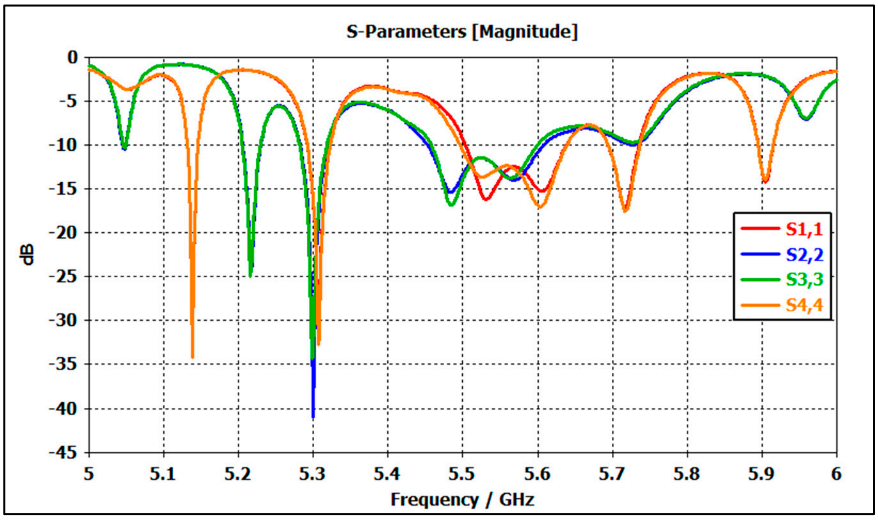

Figure 19. Reflection coefficient of the BM for all input ports (1–4) when each port is excited at a time.

The proposed antenna, depicted in Figure 9, steers the direction of the far-field radiation through a Butler Matrix (BM). This antenna design enables the transmission of beams in four distinct directions, which is a key characteristic of Butler matrix-fed arrays used for beamforming and steering applications [93]. The antenna can be conveniently mounted on the roof of an underground mine tunnel. When a mobile device, such as a miner or a vehicle, enters the antenna's range, the BM automatically steers the beam to track the device's movement within the tunnel. For instance, if a signal is fed to port 1 of the antenna and a wireless device worn by the miner connects to the beam in the direction of 27°, the antenna continuously tracks the device as it moves along the tunnel. Once the miner moves out of the range of beam 1, the connection switches to beam 4, fed by port 4, at an angle of 16°. Likewise, beam 3 connects to the device at −12°, and beam 2 provides coverage at −26°, as shown in Figure 21. This dynamic beam steering capability, common in BM-based systems, allows for seamless connectivity and tracking in confined environments like tunnels [97]. This approach also significantly reduces multipath signals, enhancing the signal-to-noise ratio and minimizing interference compared to traditional omnidirectional antennas. Additionally, the antenna exhibits circular polarization characteristics, which help mitigate polarization mismatches and enhance signal strength, a feature that is especially advantageous in environments prone to signal degradation due to physical obstructions [98].

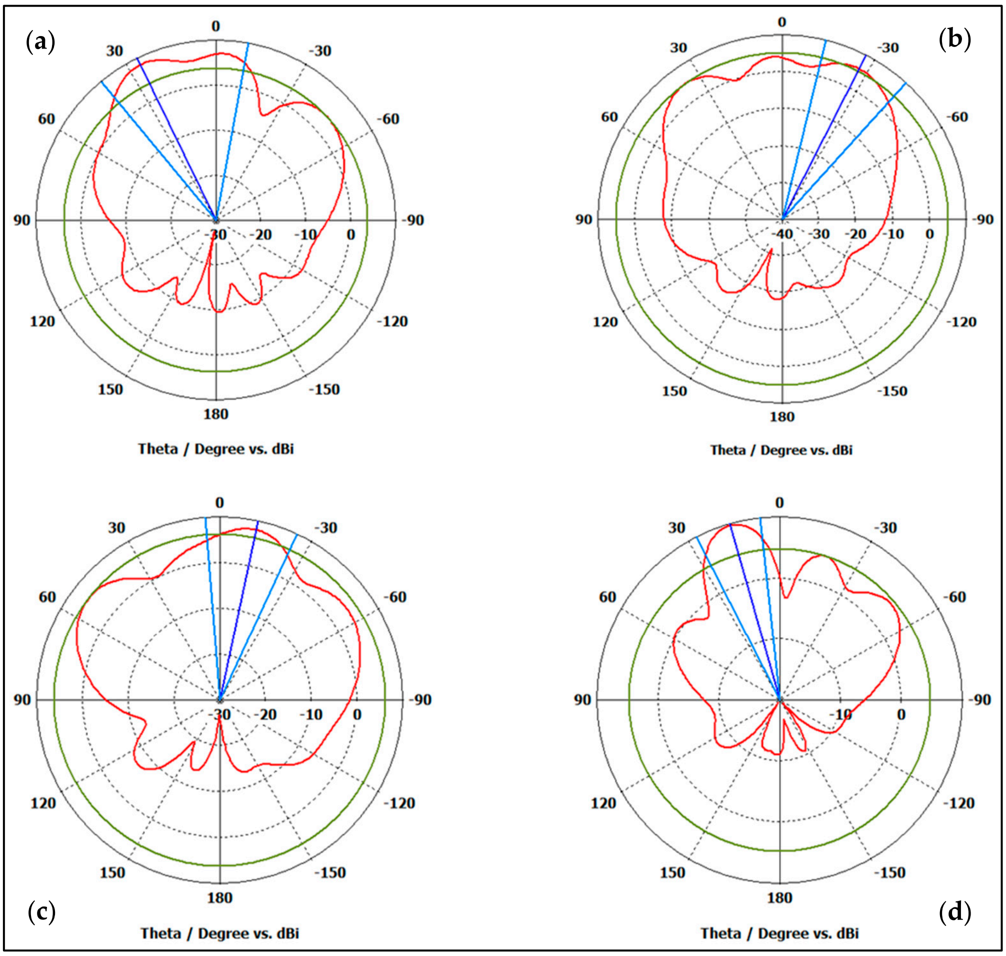

Figure 20. Far-field radiation pattern of the proposed antenna with Butler matrix when (**a**) port 1, (**b**) port 2, (**c**) port 3, and (**d**) port 4 are excited.

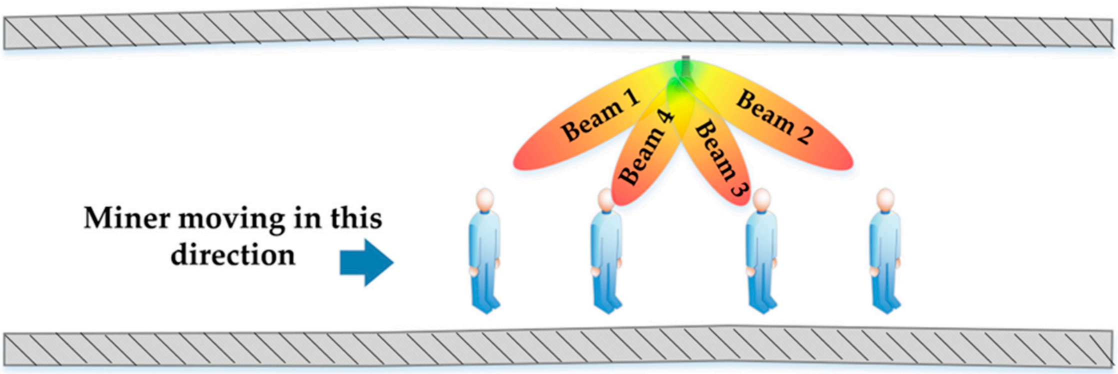

Figure 21. Visualization of the miner with beam steering of the antenna.

The proposed antenna's performance can be compared to previous studies, demonstrating its advancements in both beam steering and polarization capabilities. For instance, Harrington [99], discussed a monopole array capable of beam steering, but its design was limited to only four specific angles (−45°, −15°, 15°, and 45°). While this early work contributed to the development of beam steering technologies, the monopole array lacked the flexibility and sophistication needed for complex environments like underground mines. The absence of circular polarization in Harrington's monopole array constrained its adaptability in environments prone to signal reflections and polarization mismatches, which are frequent in underground mining as indicated by Hu et al. [100]. Similarly, Singh and Tripathi [101] presented a rectangular patch array with beam steering at the same four angles. However, their work did not consider waveform polarization or propose an antenna structure that could handle circular polarization. In dynamic environments where signal reflections are common, circular polarization is essential for minimizing polarization mismatches, thus maintaining consistent signal strength. Without circular polarization, their rectangular patch array faced limitations in its ability to handle complex signal environments, unlike the proposed antenna, which offers beam steering along with circular polarization capabilities [102] (Huang & Liu, 2022). Additionally, Seddiki et al. [103] described a dipole antenna array with beamforming capabilities, but their array was limited by its linear polarization. Linear polarization, while useful in some applications, is particularly vulnerable to signal loss and interference when there are multiple reflections or obstructions. This is especially true in underground mining environments, where the signal is likely to encounter various obstacles such as rock walls. Linear polarization often results in degraded signal quality under such conditions, while circular polarization offers greater robustness against these challenges. The proposed antenna, by leveraging circular polarization, ensures stronger signal integrity in these challenging conditions and provides superior performance compared to the dipole arrays used in previous studies [104].

The key distinguishing factor of the proposed antenna lies in its dual functionality, combining beam steering with circularly polarized waveforms. This feature is especially valuable in underground mining, where maintaining reliable communication with moving targets, such as miners or vehicles, is essential. The antenna's ability to dynamically steer its beams toward specific angles ensures continuous connectivity while reducing the likelihood of signal degradation due to polarization mismatches. Unlike the monopole, rectangular patch, and dipole arrays discussed in previous studies, the proposed antenna can adapt its signal to both user movement and environmental conditions, ensuring enhanced performance and communication reliability [97]. The performance of the proposed antenna was evaluated against existing designs reported in the literature to emphasize its distinct advantages. Table 7 presents a comparative analysis of critical performance parameters. The results indicate that the proposed antenna outperforms its counterparts, particularly in gain, bandwidth, and circular polarization, making it highly effective for the demanding conditions of underground mining applications.

Furthermore, the antenna's installation simplicity is crucial for industries like mining, where rapid deployment is critical to minimize downtime. Its compact size and straightforward installation process, such as mounting on a pole or bracket, make it ideal for confined spaces, allowing for efficient and flexible deployment. This combination of advanced beam steering, circular polarization, and ease of installation makes the proposed antenna a highly effective solution for maintaining reliable communication in underground mining environments. The generalized illustration of the proposed single-element square patch antenna with circular polarization and beam steering is given in Figure 22. The circular polarization is a key feature that allows for the antenna to transmit and receive signals in all directions, which is essential in environments like underground mines where obstacles such as rocks and walls can disrupt communication. Circularly polarized antennas are particularly beneficial in such scenarios, as they reduce signal degradation caused by polarization mismatches [102]. Another important characteristic of this antenna is beam steering, which enables it to direct its signal toward specific directions, an advantage when multiple users or obstructions are present in the region. Beam steering in antenna systems is a well-documented solution for overcoming interference and multipath effects in confined environments [105]. The ease of installation of the single-element square patch antenna with circular polarization and beam steering is crucial in industries like mining, where downtime can be costly. The compact size and simple installation process, such as mounting on a pole or bracket, make it suitable for confined areas, ensuring effective and reliable communication.

Table 7. Performance comparison of designed antenna with existing antennas.

Reference/Antenna	Frequency Range (GHz)	Bandwidth	Gain (dBi)	Polarization	Beam Steering	Primary Focus/Application	Notes/Suitability
Proposed (this work)	5.52–5.99	400 MHz	9.69	Circular	Yes	Underground mining	Enhanced reliability, minimized interference, and robust coverage.
El Azhari, Talbi, Arabi, Nedil, Seddiki, and Kandil [19]	2.45	200 MHz	7.50	Circular	No	General communication	Focus on reducing polarization mismatch; no beam steering.
Kunsei, Bialkowski, Alam, and Abbosh [29]	–	0.58 GHz (580 MHz)	8.50	Linear	No	General	Lower design complexity; does not target mining-specific challenges.
Chandra Dash, Nagalakshmaiah, Reddy, and Mukherjee [32]	0.058	Narrow	3.43	-	-	Emergency communication	Electrically small; suitable for wearable or ultra-compact applications.
Laribi, Hakem, and Elkarkraoui [36]	58–68	~1000 MHz (1 GHz)	11.20	Circular	No	mmWave applications	High data rates; can be used in select high-frequency underground systems.
Coulibaly, Nedil, Talbi, and Denidni [39]	59.55	255 MHz	15.40	Linear	Limited	Underground applications	High-gain DRA; beam steering capability is restricted.
Agouzoul, Nedil, Coulibaly, Denidni, Mabrouk, and Talbi [40]	–	0.38 GHz (380 MHz)	10.70	Circular	Yes	Mining tunnels	High design complexity; addresses multipath in confined environments.
Chen and Elsherbeni [46]	0.915	Narrow	5.00	–	–	Localization	RFID-based approach; suitable for tracking in constrained areas.
Chaouche, Nedil, Mabrouk, and Belazzoug [48]	2.45 and 5.8	500 MHz (dual-band)	8.40	Linear (dual-band)	No	General/moderate for underground	Limited gain at lower frequencies; may require additional optimization.
Kamil, Coulibaly, Adnane, Nedil, and Denidni [49]	2.51–4.90	Moderate	8.78	–	–	Multi-frequency applications	Versatile across several bands; not specifically tailored for mining.
Habani, Nedil, Denidni, and Talbi [50]	5.8	150 MHz	8.00	Linear	No	Wearable mining devices	Designed for off-body usage; suitable for worker safety monitoring.
Regev, Zolkov, and Cohen [77]	5.5	300 MHz	8.50	Linear	Yes	General communication	Uses a hybrid BLC approach for beam steering; not strictly for mining.
Seddiki, Nedil, and Ghanem [103]	–	0.45 GHz (450 MHz)	8.20	Circular	Yes	Mining tunnels	Moderate design complexity; beam steering aids in mitigating dead zones.

Reliable communication is critical in underground mining to ensure miner safety and the effectiveness of mining operations. Even in the most difficult underground settings, the single-element square patch antenna delivers dependable transmission. The circular polarization and beam steering capabilities ensure a strong and reliable signal, decreasing the possibility of interference or signal loss, which is essential in environments like underground mines where communication is often disrupted by obstacles such as rock formations and walls [106]. Moreover, by transmitting electromagnetic signals exclusively in desired directions and increasing the antenna system's gain, the implementation of a smart antenna system holds the potential to significantly decrease power consumption in underground mine communication. Smart antenna systems have been shown to optimize energy efficiency and reduce interference, which is particularly beneficial for applications such as wearable devices, where low power consumption can extend battery life [107,108]. The usage of smart antenna systems in underground mines has been demonstrated to improve communication reliability, extend coverage range, and reduce power consumption. This is particularly important for battery-operated devices such as miners' wearable sensors or communication tools, which benefit from extended battery life due to the lower power demands of the system. The beam steering technique provides a generalized solution for various underground applications by reducing signal interference and improving the signal-to-noise ratio, even in complex and dynamic environments like underground tunnels. By directing the antenna's radiation pattern toward specific areas, the communication system becomes more efficient and effective, leading to improved connectivity and operational reliability, as also reported by [109,110]. However, while the proposed antenna with beam steering characteristics is effective in reducing signal interference, the Butler matrix used provides only four fixed beams on its output, which may limit flexibility compared to more advanced, fully adaptive beamforming technologies that allow for continuous steering across a broader range of angles [111]. Despite this limitation, the proposed design remains highly effective for specific underground applications where fixed beam angles are sufficient, and its low power consumption and robust performance make it well-suited for improving communication systems in underground mining environments [112].

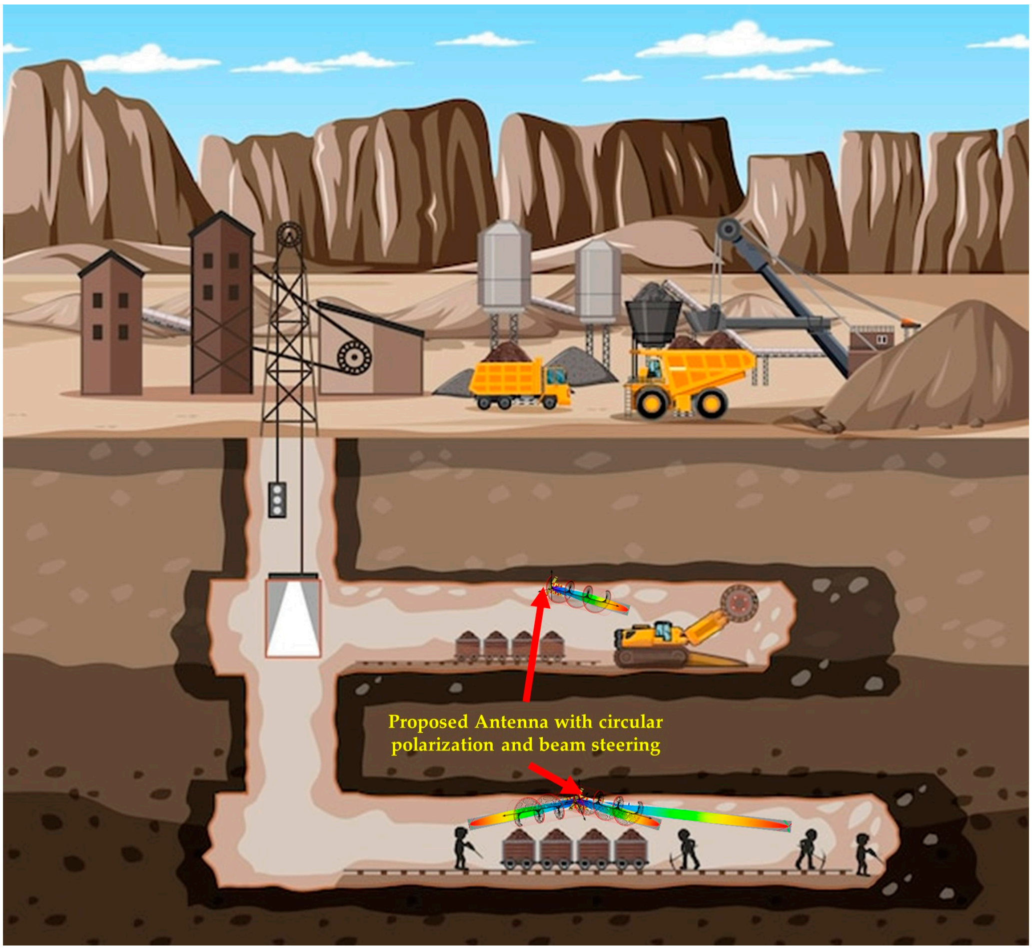

Figure 22. The general architecture of the proposed single-element square patch antenna with circular polarization and beam steering.

4. Conclusions

This study presents a significant advancement in underground mining communication systems by proposing a smart antenna system that integrates circular polarization and beam steering. The four-element square patch array, paired with a Butler matrix for beamforming, demonstrates improved signal coverage, interference mitigation, and adaptability to the harsh underground environment. The system's performance, operating within the 5.52–5.99 GHz range with a 400 MHz bandwidth and gain of up to 9.69 dBi, highlights its potential for reliable communication through precise directional control. The integration of circular polarization resolves polarization mismatches, ensuring consistent signal transmission in multipath fading environments. Beam steering further enhances performance by directing signals efficiently, minimizing dead zones and interference, which is crucial for both safety and operational efficiency in mining operations. Future research could focus on several areas to further optimize and expand the functionality of the proposed system: (i) explore the use of advanced materials, such as graphene and metamaterials, to improve antenna performance; (ii) miniaturize antenna elements and integrate beam steering functionalities into more compact form factors, allowing for deployment in space-constrained environments such as underground mines; (iii) enhance frequency agility and bandwidth to support multi-frequency or wideband operation, making the system compatible with various wireless communication standards and services; (iv) integrate intelligent features like cognitive radio capabilities, machine learning algorithms, and adaptive signal processing techniques to improve the antenna system's adaptability in dynamic environments; (v) develop energy-efficient designs, including low-power phase-shifting components, power-aware beam steering algorithms, and energy harvesting technologies to extend the system's operational lifespan. The proposed smart antenna system, with its potential future enhancements, offers a robust, scalable solution for improving communication reliability and efficiency in underground mining and other challenging environments.

Author Contributions: Conceptualization, M.A.M., I.A., and H.I.; methodology, M.A.M., M.A.A., G.T.N., and I.A.; formal analysis, M.A.M., I.A., and M.A.A.; investigation, M.A.M. and M.A.A.; resources, I.A. and G.T.N.; writing—original draft preparation, M.A.M., M.A.A., and I.A.; writing—review and editing, M.A.M., M.A.A., I.A., H.I., G.T.N., J.Q., A.M., I.K., B.G., and B.M.; visualization, M.A.A., I.A., B.G., B.M., and I.K.; funding acquisition, M.A.M. All authors have read and agreed to the published version of the manuscript.

Funding: This research received no external funding.

Data Availability Statement: The raw data supporting the conclusions of this article will be made available by the authors on request.

Acknowledgments: The authors would like to acknowledge the Sibanye-Stillwater Digital Mining laboratory (DigiMine) at the Wits Mining Institute (WMI), University of the Witwatersrand, Johannesburg, for providing the resources necessary to conduct this research.

Conflicts of Interest: The authors declare no conflicts of interest.

References

1. Рудько, Г. The role of mining industry in the world economy and the economy of Ukraine. *Мінеральні Ресурси України* **2019**, 23–29. [CrossRef]
2. Singh, A.; Kumar, D.; Hötzel, J. IoT Based information and communication system for enhancing underground mines safety and productivity: Genesis, taxonomy and open issues. *Ad Hoc Netw.* **2018**, *78*, 115–129. [CrossRef]
3. Misra, P.; Kanhere, S.; Ostry, D.; Jha, S. Safety assurance and rescue communication systems in high-stress environments: A mining case study. *IEEE Commun. Mag.* **2010**, *48*, 66–73. [CrossRef]
4. Pattnaik, S.K.; Samal, S.R.; Bandopadhaya, S.; Swain, K.; Choudhury, S.; Das, J.K.; Mihovska, A.; Poulkov, V. Future wireless communication technology towards 6g IoT: An application-based analysis of IoT in real-time location monitoring of employees inside underground mines by using BLE. *Sensors* **2022**, *22*, 3438. [CrossRef]
5. Yarkan, S.; Guzelgoz, S.; Arslan, H.; Murphy, R.R. Underground mine communications: A survey. *IEEE Commun. Surv. Tutor.* **2009**, *11*, 125–142. [CrossRef]

6. Carreras-Coch, A.; Navarro, J.; Sans, C.; Zaballos, A. Communication technologies in emergency situations. *Electronics* **2022**, *11*, 1155. [CrossRef]
7. Shabina, S. Smart helmet using RF and WSN technology for underground mines safety. In Proceedings of the 2014 International Conference on Intelligent Computing Applications, Coimbatore, India, 6–7 March 2014; pp. 305–309.
8. Bandyopadhyay, L.; Chaulya, S.; Mishra, P. Wireless Communication in Underground Mines. In *RFID-Based Sensor Networking*; Springer: New York, NY, USA, 2010; Volume 22.
9. Radinovic, G.; Kim, K. Feasibilty study of RFID/Wi-Fi/BlueTooth wireless tracking system for underground mine mapping–Oklahoma. In Proceedings of the Incorporating Geospatial Technologies into SMCRA Business Processes, Atlanta, GA, USA, 25–27 March 2008.
10. Murphy, J.N.; Parkinson, H.E. Underground mine communications. *Proc. IEEE* **1978**, *66*, 26–50. [CrossRef]
11. Toro, U.S.; ElHalawany, B.M.; Wong, A.B.; Wang, L.; Wu, K. Backscatter communication-based wireless sensing (BBWS): Performance enhancement and future applications. *J. Netw. Comput. Appl.* **2022**, *208*, 103518. [CrossRef]
12. Javaid, F.; Wang, A.; Sana, M.U.; Husain, A.; Ashraf, I. An optimized approach to channel modeling and impact of deteriorating factors on wireless communication in underground mines. *Sensors* **2021**, *21*, 5905. [CrossRef]
13. Ranjan, A.; Sahu, H.; Sahu, H. Communications challenges in underground mines. *Communications* **2014**, *5*, 23–29.
14. Li, L.; Vuran, M.C.; Akyildiz, I.F. Characteristics of underground channel for wireless underground sensor networks. *Proc. Med-Hoc-Net* **2007**, *7*, 13–15.
15. Jacksha, R.; Zhou, C.; Sunderman, C. Measurement of the Influence of Antennas on Radio Signal Propagation in Underground Mines and Tunnels. *Prog. Electromagn. Res. C. Pier C* **2019**, *94*, 1. [CrossRef]
16. Neto, A.S.e.S.; de Araujo Farias, G.; da Silva, D.O.; de Oliveira, A.L.T.; de Paula Dias Queiroz, A. Cylindrical Rectangular Antenna for Wireless Communications. In *New Contributions in Information Systems and Technologies*; Springer International Publishing: Cham, Switzerland, 2015; Volume 2, pp. 21–31.
17. Yu, Z.; Teng, J.; Bai, X.; Xuan, D.; Jia, W. Connected coverage in wireless networks with directional antennas. *ACM Trans. Sens. Netw. (TOSN)* **2014**, *10*, 1–28. [CrossRef]
18. Sun, H.; Sun, S. A novel reconfigurable feeding network for quad-polarization-agile antenna design. *IEEE Trans. Antennas Propag.* **2015**, *64*, 311–316. [CrossRef]
19. El Azhari, M.E.H.; Talbi, L.; Arabi, L.; Nedil, M.; Seddiki, M.L.; Kandil, N. Channel characterization of circularly polarized antenna MIMO system in an underground mine. *Prog. Electromagn. Res. M* **2018**, *67*, 9–19. [CrossRef]
20. Bei, L.; Zhang, L.; Huang, K. A novel microstrip array circular polarized antenna based on t-type power divider. *Wirel. Netw.* **2021**, 1–7. [CrossRef]
21. Forooshani, A.E.; Bashir, S.; Michelson, D.G.; Noghanian, S. A survey of wireless communications and propagation modeling in underground mines. *IEEE Commun. Surv. Tutor.* **2013**, *15*, 1524–1545. [CrossRef]
22. Mabrouk, I.B.; Talbi, L.; Nedil, M.; Coulibaly, Y.; Denidni, T. Effect of antenna directivity on performance of multiple input multiple output systems in an underground gold mine. *IET Microw. Antennas Propag.* **2012**, *6*, 555–561. [CrossRef]
23. El Azhari, M.E.H.; Nedil, M.; Mabrouk, I.B.; Ghanem, K.; Talbi, L. Characterization of an off-body channel at 2.45 GHz in an underground mine environment. *Prog. Electromagn. Res. M* **2015**, *43*, 91–100. [CrossRef]
24. Chaudhary, R.K. A Compact Rectangular Ring Antenna with Meander Line for UHF Band Communications. In Proceedings of the 2022 IEEE Microwaves, Antennas, and Propagation Conference (MAPCON), Bangalore, India, 12–16 December 2022; pp. 635–639.
25. Nedil, M.; Habib, A.; Djaiz, A.; Denidni, T. Novel ultra-wideband Butler matrix for wireless underground mines. In Proceedings of the 2010 IEEE Antennas and Propagation Society International Symposium, Toronto, ON, Canada, 11–17 July 2010; pp. 1–4.
26. Chen, A.; Ning, X. A pattern and polarization reconfigurable antenna with metasurface. *Int. J. RF Microw. Comput.-Aided Eng.* **2021**, *31*, e22312. [CrossRef]
27. Zhang, Y.; Gu, P.; Xu, J.; Ding, D. A Design of a multi parameter reconfigurable array antenna. In Proceedings of the 2022 International Applied Computational Electromagnetics Society Symposium (ACES-China), Xuzhou, China, 9–12 December 2022; pp. 1–3.
28. Hu, J.; Yang, X.; Ge, L.; Guo, Z.; Hao, Z.-C.; Wong, H. A reconfigurable 1×4 circularly polarized patch array antenna with frequency, radiation pattern, and polarization agility. *IEEE Trans. Antennas Propag.* **2021**, *69*, 5124–5129. [CrossRef]
29. Kunsei, H.; Bialkowski, K.S.; Alam, M.S.; Abbosh, A.M. Improved communications in underground mines using reconfigurable antennas. *IEEE Trans. Antennas Propag.* **2018**, *66*, 7505–7510. [CrossRef]
30. Tamim, A.M.; Faruque, M.R.; Islam, M.T. Metamaterial-inspired electrically small antenna for microwave applications. *Proc. Inst. Mech. Eng. Part L: J. Mater. Des. Appl.* **2022**, *236*, 2230–2241. [CrossRef]
31. Kishor, T.; Griffin, A.A.; Paul, C.J.; Neebha, T.M.; Andrushia, A.D.; Bruntha, P.M. Design and Analysis of Electrically Small 915MHz Antenna for Wireless Applications. In Proceedings of the 2021 3rd International Conference on Signal Processing and Communication (ICPSC), Coimbatore, India, 13–14 May 2021; pp. 281–284.

32. Chandra Dash, J.; Nagalakshmaiah, K.; Reddy, G.S.; Mukherjee, J. Electrically small hemi-cylindrical-shaped multilayered very high frequency antenna for underground mine communication. *IET Microw. Antennas Propag.* **2020**, *14*, 491–497. [CrossRef]
33. Roestorff, M. Design of an Electronically Small Wearable Antenna with a Reactive Impedance Substrate Operating at 433 MHz. Master's Thesis, University of Pretoria, Pretoria, South Africa, 2017.
34. Mohamed, H.A.; Edries, M.; Abdelghany, M.A.; Ibrahim, A.A. Millimeter-wave antenna with gain improvement utilizing reflection FSS for 5G networks. *IEEE Access* **2022**, *10*, 73601–73609. [CrossRef]
35. Pramono, S.; Suharjono, A.; Wardihani, E.D.; Mara, M.N.; Mukhlisin, M. A Compact Enhanced Bandwidth Slotted Millimeter Wave Microstrip Patch Antenna for 5G Wireless Application. In Proceedings of the 2023 International Conference on Informatics, Multimedia, Cyber and Informations System (ICIMCIS), Jakarta Selatan, Indonesia, 7–8 November 2023; pp. 573–577.
36. Laribi, M.; Hakem, N.; Elkarkraoui, T. Hight-gain circularly polarized multilayer dielectric resonator antenna for millimeter-wave application. In Proceedings of the 2017 IEEE International Symposium on Antennas and Propagation & USNC/URSI National Radio Science Meeting, San Diego, CA, USA, 9–14 July 2017; pp. 1523–1524.
37. Liu, X.; Yin, X.; Zheng, G. Experimental investigation of millimeter-wave MIMO channel characteristics in tunnel. *IEEE Access* **2019**, *7*, 108395–108399. [CrossRef]
38. Hu, Z.; Zhao, H.; Kraman, M.; Huang, W.; Tu, H.; Sang, L. A beam-steering antenna with low deflecting-loss enabled by a miniaturized flexible lens. *J. Electromagn. Waves Appl.* **2023**, *37*, 730–751. [CrossRef]
39. Coulibaly, Y.; Nedil, M.; Talbi, L.; Denidni, T. High gain cylindrical dielectric resonator with superstrate for broadband millimeter-wave underground mining communications. In Proceedings of the 2010 14th International Symposium on Antenna Technology and Applied Electromagnetics & the American Electromagnetics Conference, Ottawa, ON, Canada, 5–8 July 2010; pp. 1–4.
40. Agouzoul, A.; Nedil, M.; Coulibaly, Y.; Denidni, T.; Mabrouk, I.B.; Talbi, L. Design of a high gain hybrid dielectric resonator antenna for millimeter-waves underground applications. In Proceedings of the 2011 IEEE International Symposium on Antennas and Propagation (APSURSI), Spokane, WA, USA, 3–8 July 2011; pp. 1688–1691.
41. Chorfi, H.; Nedil, M.; Coulibaly, Y.; Denidni, T.A.; Mabrouk, I.B.; Talbi, L. A dielectric resonator antenna mounted on a conformal structure at 60 GHz. In Proceedings of the 2011 IEEE International Symposium on Antennas and Propagation (APSURSI), Spokane, WA, USA, 3–8 July 2011; pp. 2577–2580.
42. Chorfi, H.; Nedil, M.; Mabrouk, I.B.; Denidni, T.; Talbi, L. Design of a 60 GHz dielectric resonator antenna array mounted on a conformal structure. In Proceedings of the Proceedings of the 2012 IEEE International Symposium on Antennas and Propagation, Chicago, IL, USA, 8–14 July 2012; pp. 1–2.
43. Erman, F.; Koziel, S.; Hanafi, E.; Soboh, R.; Szczepanski, S. Miniaturized metal-mountable U-shaped inductive-coupling-fed UHF RFID tag antenna with defected microstrip surface. *IEEE Access* **2022**, *10*, 47301–47308. [CrossRef]
44. Lopez, Z.Y.; Akhter, Z.; Shamim, A. 3D printed RFID tag antenna miniaturized through volumetric folding and slow-wave structures. *IEEE J. Radio Freq. Identif.* **2022**, *6*, 164–175. [CrossRef]
45. Hautcoeur, J.; Talbi, L.; Nedil, M. High gain RFID tag antenna for the underground localization applications at 915 MHz band. In Proceedings of the 2013 IEEE Antennas and Propagation Society International Symposium (APSURSI), Orlando, FL, USA, 7–13 July 2013; pp. 1488–1489.
46. Chen, Y.; Elsherbeni, A.Z. Circularly polarized RFID tag antenna design for underground localization system. In Proceedings of the 2021 United States National Committee of URSI National Radio Science Meeting (USNC-URSI NRSM), Boulder, CO, USA, 4–9 January 2021; pp. 205–206.
47. Meng, W.; Gu, Y.; Bao, J.; Lian, Z.; Kong, Z.; Yin, W. Spatially Modulated Sparse Code Multiple Access in Uplink Mine Communications. In Proceedings of the 2022 13th Asian Control Conference (ASCC), Jeju, Republic of Korea, 4–7 May 2022; pp. 1660–1664.
48. Chaouche, Y.B.; Nedil, M.; Mabrouk, I.B.; Belazzoug, M. A dual-band antenna backed by AMC surface using genetic algorithm for 2.4/5.8 GHz underground mining communications. In Proceedings of the 2020 IEEE International Symposium on Antennas and Propagation and North American Radio Science Meeting, Toronto, ON, Canada, 5–10 July 2020; pp. 929–930.
49. Kamil, A.; Coulibaly, Y.; Adnane, H.; Nedil, M.; Denidni, T.A. Design of an ultrawideband ring patch using coplanar waveguide technology for underground mining communications. In Proceedings of the 2011 24th Canadian Conference on Electrical and Computer Engineering (CCECE), Niagara Falls, ON, Canada, 8–11 May 2011; pp. 000845–000848.
50. Habani, A.; Nedil, M.; Denidni, T.A.; Talbi, L. High gain enhancement off-body antenna for underground mining communications. In Proceedings of the 2017 IEEE International Symposium on Antennas and Propagation & USNC/URSI National Radio Science Meeting, San Diego, CA, USA, 9–14 July 2017; pp. 2167–2168.
51. Habani, A.; Nedil, M.; Elazhari, M.; Ghanem, F. High gain off-body antenna based on combination AMC-FSS structure for underground mining communications. In Proceedings of the 2016 IEEE International Symposium on Antennas and Propagation (APSURSI), Fajardo, PR, USA, 26 June–1 July 2016; pp. 267–268.

52. Vallappil, A.K.; Rahim, M.K.A.; Khawaja, B.A.; Murad, N.A.; Mustapha, M.G. Butler matrix based beamforming networks for phased array antenna systems: A comprehensive review and future directions for 5G applications. *IEEE Access* **2020**, *9*, 3970–3987. [CrossRef]
53. Denidni, T.A.; Libar, T.E. Wide band four-port Butler matrix for switched multibeam antenna arrays. In Proceedings of the 14th IEEE Proceedings on Personal, Indoor and Mobile Radio Communications, PIMRC 2003, Beijing, China, 7–10 September 2003; pp. 2461–2464.
54. Angeletti, P.; Lisi, M. Multimode beamforming networks for space applications. *IEEE Antennas Propag. Mag.* **2014**, *56*, 62–78. [CrossRef]
55. Hall, P.; Vetterlein, S. Review of radio frequency beamforming techniques for scanned and multiple beam antennas. *IEE Proc. H (Microw. Antennas Propag.)* **1990**, *137*, 293–303. [CrossRef]
56. Vashist, S.; Soni, M.; Singhal, P. A review on the development of Rotman lens antenna. *Chin. J. Eng.* **2014**, *2014*, 385385. [CrossRef]
57. Méndez-Rial, R.; Rusu, C.; González-Prelcic, N.; Alkhateeb, A.; Heath, R.W. Hybrid MIMO architectures for millimeter wave communications: Phase shifters or switches? *IEEE Access* **2016**, *4*, 247–267. [CrossRef]
58. Mandloi, M.S.; Gupta, P.; Parmar, A.; Malviya, P.; Malviya, L. Beamforming MIMO array antenna for 5G-millimeter-wave application. *Wirel. Pers. Commun.* **2023**, *129*, 153–172. [CrossRef]
59. Pham, N.T.; Lee, G.-A.; De Flaviis, F. Microstrip antenna array with beamforming network for WLAN applications. In Proceedings of the 2005 IEEE Antennas and Propagation Society International Symposium, San Diego, CA, USA, 5–12 July 2005; pp. 267–270.
60. Moubadir, M.; Bayjja, M.; Touhami, N.A.; Aghoutane, M.; Tazon, A. Design and implementation of a technology planar 8 × 8 butler matrix with square truncated edge-fed array antenna for WLAN networks application. In Proceedings of the 2015 International Conference on Wireless Networks and Mobile Communications (WINCOM), Marrakech, Morocco, 20–23 October 2015; pp. 1–5.
61. Pozar, D.M. *Microwave Engineering*; Johnwiley & Sons Inc.: New York, NY, USA, 1998; pp. 367–368.
62. Yu, Z.-Y.; Zhang, Y.-H.; He, S.-Y.; Gao, H.-T.; Chen, H.-T.; Zhu, G.-Q. A wide-angle coverage and low scan loss beam steering circularly polarized folded reflectarray antenna for millimeter-wave applications. *IEEE Trans. Antennas Propag.* **2021**, *70*, 2656–2667. [CrossRef]
63. Huang, C.; Pan, W.; Luo, X. Low-loss circularly polarized transmitarray for beam steering application. *IEEE Trans. Antennas Propag.* **2016**, *64*, 4471–4476. [CrossRef]
64. Sharifi, G.; Zehforoosh, Y.; Sedghi, T.; Takrimi, M. Circularly polarized beam steering array antenna fed by low magnitude and phase error response of Butler matrix to use pattern stabilization applications. *Int. J. RF Microw. Comput. -Aided Eng.* **2022**, *32*, e23022. [CrossRef]
65. Islam, M.T.; Imran, A.Z.M.; Chowdhury, F.; Hridoy, M.N.N.; Kabir, M.H.; Gafur, A.; Rashid, S.Z. Design and Analysis of Multiband Microstrip Patch Antenna Array for 5G Communications. In Proceedings of the 2022 International Conference on Innovations in Science, Engineering and Technology (ICISET), Chittagong, Bangladesh, 25–28 February 2022; pp. 29–32.
66. Sun, X.L.; Liu, L.; Cheung, S.; Yuk, T. Dual-band antenna with compact radiator for 2.4/5.2/5.8 GHz WLAN applications. *IEEE Trans. Antennas Propag.* **2012**, *60*, 5924–5931. [CrossRef]
67. Bodhaye, N.A.; Zade, P.L. Design of Multi-band Double I-shaped slot Microstrip Patch Antenna With Defected Ground Structure for Wireless Application. *IOSR J. Electron. Commun. Eng. (IOSR-JECE) E-ISSN* **2018**, *13*, 2278–2834.
68. Neelima, K.; Divya, N.; Karthikeyan, K.; Kumar, N. Design of Rubber Substrate based Flexible Antenna with DGS for WBAN Applications. In Proceedings of the 2022 International Conference on Emerging Smart Computing and Informatics (ESCI), Pune, India, 9–11 March 2022; pp. 1–4.
69. He, M.; Ye, X.; Zhou, P.; Zhao, G.; Zhang, C.; Sun, H. A small-size dual-feed broadband circularly polarized U-slot patch antenna. *IEEE Antennas Wirel. Propag. Lett.* **2014**, *14*, 898–901. [CrossRef]
70. Scarselli, C.; Pascarella, F.; Ciampalini, C.; Nenna, G.; Monorchio, A. Compact Slot-Patch Antenna with Dual Circular Polarization. In Proceedings of the 2023 IEEE International Symposium on Antennas and Propagation and USNC-URSI Radio Science Meeting (USNC-URSI), Portland, OR, USA, 23–28 July 2023; pp. 907–908.
71. Fadhil, T.Z.; Hamid, M.R.; Murad, N.A.; Rahim, M.K.A. Circularly Polarized Patch Antenna with Rotated S Shape Slot For 5 G Application. In Proceedings of the 2022 International Symposium on Antennas and Propagation (ISAP), Sydney, Australia, 31 October–3 November 2022; pp. 145–146.
72. Nayak, A.K.; Chouhan, M.; Moez, K.; Kartikeyan, M.; Patnaik, A. Dual-Band Substrate Integrated Waveguide (SIW) Cavity Slot Antenna for C-Band Applications. In Proceedings of the 2022 IEEE Microwaves, Antennas, and Propagation Conference (MAPCON), Bangalore, India, 12–16 December 2022; pp. 1302–1307.
73. Hassan, Y.; Rolny, R.T.; Wittneben, A. MIMO relaying with compact antenna arrays: Coupling, noise correlation and superdirectivity. In Proceedings of the 2013 IEEE 24th Annual International Symposium on Personal, Indoor, and Mobile Radio Communications (PIMRC), London, UK, 23–28 July 2013; pp. 10710–11076.

74. Chen, X.; Pei, H.; Li, M.; Huang, H.; Ren, Q.; Wu, Q.; Zhang, A.; Kishk, A.A. Revisit to mutual coupling effects on multi-antenna systems. *J. Commun. Inf. Netw.* **2020**, *5*, 411–422. [CrossRef]
75. Lin, Y.-S.; Chang, J.-F.; Yeh, P.-T. Coupled-line-based millimeter-wave CMOS spiral power dividers with tapered TLs. *Analog Integr. Circuits Signal Process.* **2021**, *109*, 625–637. [CrossRef]
76. Wang, X.; Yang, S.; Lu, G. Compensation Approach for Miniaturized Wilkinson Power Divider Design. In Proceedings of the 2022 Asia-Pacific Microwave Conference (APMC), Yokohama, Japan, 29 November–2 December 2022; pp. 16–18.
77. Regev, D.; Zolkov, E.; Cohen, E. S-Parameter Analysis and Compact Formulation of Two-Port 90° N-Path Circuits. *IEEE Trans. Circuits Syst. II: Express Briefs* **2022**, *69*, 4679–4683. [CrossRef]
78. Kouhalvandi, L.; Matekovits, L. Surrogate modeling for designing and optimizing mimo antennas. In Proceedings of the 2022 IEEE International Symposium on Antennas and Propagation and USNC-URSI Radio Science Meeting (AP-S/URSI), Denver, CO, USA, 10–15 July 2022; pp. 1540–1541.
79. DiLullo, C.; Reeve, W.D.; Hicks, B.C.; Dowell, J. Scattering Parameter Measurements of the Long Wavelength Array Antenna and Front End Electronics. *Publ. Astron. Soc. Pac.* **2023**, *135*, 044501. [CrossRef]
80. Liu, L.; Chen, K.; Wu, Z.-J.; Wang, Z.-B. Filtering Phase Shifters Using Vertically Installed Planar Structure. In Proceedings of the 2022 IEEE MTT-S International Wireless Symposium (IWS), Harbin, China, 12–15 August 2022; pp. 1–3.
81. Xu, W.; Li, T.; Chen, X.; Chen, H.; Feng, L. Highly selective phase shifter using stub-loaded coupled-line resonators. *Microw. Opt. Technol. Lett.* **2023**, *65*, 3164–3170. [CrossRef]
82. Tian, C.; Dai, C.; Ju, L.; Wang, C. Dual Polarization Filter Antenna Based on Slots. In Proceedings of the 2023 International Conference on Microwave and Millimeter Wave Technology (ICMMT), Qingdao, China, 14–17 May 2023; pp. 1–3.
83. Hamzah, S.; Malek, N.; Isa, F.; Mohammad, S.; Azman, A.; Islam, M. Design of Dual-Linearly Polarized Patch Antenna at Millimetrewaves. In Proceedings of the 2022 IEEE International Symposium on Antennas and Propagation and USNC-URSI Radio Science Meeting (AP-S/URSI), Denver, CO, USA, 10–15 July 2022; pp. 1184–1185.
84. Sharma, M.; Kapula, P.R.; Alagrama, S.; Sharma, K.; Pandey, G.P.; Singh, D.K.; Mahajan, M.; Gupta, A. Miniaturized quad-port conformal multi-band (qpc-mb) mimo antenna for on-body wireless systems in microwave-millimeter bands. *IEEE Access* **2023**, *11*, 105982–105999. [CrossRef]
85. Schmidt, C.H.; Leibfritz, M.M.; Eibert, T.F. Fully probe-corrected near-field far-field transformation employing plane wave expansion and diagonal translation operators. *IEEE Trans. Antennas Propag.* **2008**, *56*, 737–746. [CrossRef]
86. Bendaoudi, A.; Berka, M.; Debab, M.; Mahdjoub, Z. Effects of ground plane on a square graphene ribbon patch antenna designed on a high-permittivity substrate with PBG structures. *Frequenz* **2023**, *77*, 385–394. [CrossRef]
87. Deshmukh, A.A.; Surendran, S.; Rane, A.; Bhasin, Y.; Chavali, V.A. Compact designs of circular microstrip antennas employing modified ground plane for wideband response. *AEU-Int. J. Electron. Commun.* **2024**, *176*, 155130. [CrossRef]
88. Chaabane, A.; Guerroui, M.; Aissaoui, D. Circularly polarized quasi-rectangular patch UWB antenna for GPR applications. *SJEE* **2022**, *19*, 261–271. [CrossRef]
89. Ahmed, A.S.; Kadhim, Y.J.; Abedi, F.; Almaameri, I.M. Circular Polarized Patch Antenna Minimization for 5 GHz Applications Based on Genetics Algorithm. In Proceedings of the 2022 5th International Conference on Engineering Technology and its Applications (IICETA), Al-Najaf, Iraq, 31 May–1 June 2022; pp. 498–501.
90. Supreeyatitikul, N.; Boonpoonga, A.; Phongcharoenpanich, C. Gain Enhancement of Circularly Polarized Aperture-Coupled Microstrip Patch Antenna Using Partially Reflective Surface. In Proceedings of the 2022 Joint International Conference on Digital Arts, Media and Technology with ECTI Northern Section Conference on Electrical, Electronics, Computer and Telecommunications Engineering (ECTI DAMT & NCON), Chiang Rai, Thailand, 26–28 January 2022; pp. 290–293.
91. Zakeri, H.; Parvaneh, M.; Moradi, G. A compact rhcp and lhcp truncated corner patch series-fed array antenna. *Int. J. Electron. Lett.* **2023**, *11*, 125–133. [CrossRef]
92. Van Messem, L.; Moerman, A.; Caytan, O.; de Paula, I.L.; Hoflack, B.; Stroobandt, B.; Lemey, S.; Moeneclaey, M.; Rogier, H. A 4× 4 millimeterwave-frequency Butler matrix in grounded co-planar waveguide technology for compact integration with 5G antenna arrays. *IEEE Trans. Microw. Theory Tech.* **2022**, *71*, 122–134. [CrossRef]
93. Suryana, J.; Adhianti, L. Design and Implementation of Beam Steering Using 8× 8 Butler Matrix on X-Band Array Antenna for AESA Radar. In Proceedings of the 2023 17th International Conference on Telecommunication Systems, Services, and Applications (TSSA), Lombok, Indonesia, 12–13 October 2023; pp. 1–6.
94. Jizat, N.M.; Yamada, Y.; Yusoff, Z. Multibeam Array Antenna with Compact Size Butler Matrix for Millimeter-Wave Application. *Int. J. Integr. Eng.* **2023**, *15*, 140–152. [CrossRef]
95. Chang, C.-C.; Lee, R.-H.; Shih, T.-Y. Design of a beam switching/steering Butler matrix for phased array system. *IEEE Trans. Antennas Propag.* **2009**, *58*, 367–374. [CrossRef]
96. Dong, C.; Shen, S.; Hu, Y.; Sun, L.; Ye, M.; You, Y.; Lu, Y.; Huang, J. Butler Matrix Based on Dual-Mode Transmission Lines for Millimeter Wave Dual-Polarized Applications. In Proceedings of the 2023 International Applied Computational Electromagnetics Society Symposium (ACES-China), Hangzhou, China, 15–18 August 2023; pp. 1–3.

97. Aribi, T.; Sedghi, T.; Lou, R.K.M. High gain and circularly polarized beam-switching 8 × 8 Vivaldi antenna array for X-band application. *Int. J. Microw. Wirel. Technol.* **2023**, *15*, 836–842. [CrossRef]
98. Gafarov, E.R.; Erokhin, A.A.; Salomatov, Y.P.; Strigova, Y.A.; Aleksandrin, A.M.; Vereshagin, A.N. The circular polarized antenna array for cube satellites. In Proceedings of the 2023 Radiation and Scattering of Electromagnetic Waves (RSEMW), Divnomorskoe, Russia, 26–30 June 2023; pp. 388–391.
99. Harrington, R.F. Effect of antenna size on gain, bandwidth, and efficiency. *J. Res. Nat. Bur. Stand* **1960**, *64*, 1–12. [CrossRef]
100. Hu, J.; Yang, X.; Ge, L.; Wong, H. A polarization and beam steering reconfigurable cavity-backed magneto-electric dipole antenna array using reflection-type phase shifter. *IEEE Trans. Antennas Propag.* **2021**, *70*, 296–306. [CrossRef]
101. Singh, I.; Tripathi, V. Micro strip patch antenna and its applications: A survey. *Int. J. Comp. Tech. Appl* **2011**, *2*, 1595–1599.
102. Huang, B.-B.; Liu, N.-W. A Low-Profile Circularly Polarized Antenna Array for Beam Steering. In Proceedings of the TENCON 2022—2022 IEEE Region 10 Conference (TENCON), Hong Kong, China, 1–4 November 2022; pp. 1–3.
103. Seddiki, M.; Nedil, M.; Ghanem, F. Wideband switched beam antenna array with circular polarization for undergound mines. In Proceedings of the 2016 IEEE International Symposium on Antennas and Propagation (APSURSI), Fajardo, PR, USA, 26 June–1 July 2016; pp. 433–434.
104. Yin, L.; Yang, P.; Zeng, Q.; Zhang, P.; Dong, T.; Hu, J.; Nie, Z. Low-cost, dual circularly polarized 2-bit phased array antenna at X-band. *IEEE Trans. Antennas Propag.* **2023**, *71*, 2790–2795. [CrossRef]
105. Zhao, S.; Dong, Y. Circularly polarized beam-steering microstrip leaky-wave antenna based on coplanar polarizers. *IEEE Antennas Wirel. Propag. Lett.* **2022**, *21*, 2259–2263. [CrossRef]
106. Saha, P.; Das, J.; Venkateswaran, P. Smart Beam Steering with a Slot-Loaded Miniaturized Patch Antenna. In Proceedings of the 2022 IEEE International Conference on Signal Processing and Communications (SPCOM), Bangalore, India, 11–15 July 2022; pp. 1–4.
107. Pirapaharan, K.; Ajithkumar, N.; Sarujan, K.; Fernando, X.; Hoole, P.R. Smart, Fast, and Low Memory Beam-Steering Antenna Configurations for 5G and Future Wireless Systems. *Electronics* **2022**, *11*, 2658. [CrossRef]
108. Nedil, M.; Denidni, T.; Djaiz, A.; Habib, M.A. A new ultra-wideband beamforming for wireless communications in underground mines. *Prog. Electromagn. Res. M* **2008**, *4*, 1–21. [CrossRef]
109. Honda, K.; Takakura, K.; Otsubo, Y. Smart Gateway for Healthcare Networks Based on Beam Steering Technology. *Sensors* **2023**, *23*, 2959. [CrossRef]
110. Pirapaharan, K.; Kunsei, H.; Senthilkumar, K.; Hoole, P.; Hoole, S. A single beam smart antenna for wireless communication in a highly reflective and narrow environment. In Proceedings of the 2016 International Symposium on Fundamentals of Electrical Engineering (ISFEE), Bucharest, Romania, 30 June–2 July 2016; pp. 1–5.
111. Gaire, P.; Islam, M.K.; Khan, M.R.; Chibane, C.; Bhardwaj, S. Beam Steering for Adhoc Mesh Network Wireless Power Transfer at 2.45 GHz. In Proceedings of the 2022 IEEE International Symposium on Antennas and Propagation and USNC-URSI Radio Science Meeting (AP-S/URSI), Denver, CO, USA, 10–15 July 2022; pp. 1736–1737.
112. Chilamkurthy, N.S.; Pandey, O.J.; Ghosh, A.; Cenkeramaddi, L.R.; Dai, H.-N. Low-Power Wide-Area Networks: A Broad Overview of its Different Aspects. *IEEE Access* **2022**, *10*, 81926–81959. [CrossRef]